



UNIVERSITY OF GUANAJUATO

CAMPUS IRAPUATO SALAMANCA  
DIVISION OF ENGINEERING

---

# Study of Domain Wall Dynamics under Nonlocal Spin-Transfer Torque using Heterogeneous Computing

---

BACHELOR THESIS

*A thesis to obtain bachelor degree in Bachelor of Computacional Systems  
Engineering*

*Supervisor:*

*Author:* Dr. David Claudio González

Thomas Sanchez Lengeling *Co-Supervisor:*

Dra. Maria Susana Avila Garcia

*Examiners:*

Dr. Víctor Ayala Ramírez Dr. Juan Gabriel Aviña Cervantes

Guanajuato, Mexico

April 2015

UNIVERSITY OF GUANAJUATO

## *Abstract*

Campus Irapuato Salamanca

Division of Engineering

Department of Electronic Engineering

Bachelor of Computacional Systems Engineering

### **Study of Domain Wall Dynamics under Nonlocal Spin-Transfer Torque using Heterogeneous Computing**

by Thomas Sanchez Lengeling

This work is an exploration of the role that Graphical Processing Units, also known as GPUs, can play in the acceleration of physical simulations. In particular, in the research of spintronic effects such as the dynamics of domain walls under nonlocal spin-transfer torque. Our study is relevant because it allows researchers to quantitatively test some of the effects of a phenomenon known as spin-diffusion on magnetic configurations at the nanoscale. Some of such configurations are known as domain walls. These magnetic configurations can be observed experimentally in NiFe soft nanostripes but they are really complicated to produce and image experimentally. Due to this, we use the massively parallel capabilities of a single GPU to numerically solve a mathematical equation, known as the Zhang-Li model. As a consequence of our implementation, we have observed a 8.0x speed-up in the solution of the equation. This speed-up is obtained when we compare the time needed to obtain the result of a simulation in a GPU with that of a simulation with the same input parameters in a conventional processor e.g. Intel Xeon. The numerical method used for the solution is a the method known as Finite Differences in the Time Domain (FDTD) whose integration is done using a 4th order integrator.

## *Acknowledgements*

To my advisor David Claudio for being supportive and flexible throughout the thesis endeavor, he allowed me to continue learning GPU thought various experiences.

I want to thank my family especially my parents Manuel and Martha, my two brothers Benjamin and Gabriel, as well as everyone that help me through the process. Karen who encourage me to finish fast and stop playing DOTA.

All my bachelor colleagues, we survived together through the courses, projects and work, and all the friends that I made along the way. Finally, to the University of Guanajuato for the support and assistance in the process. I had numerous experiences at the University that will allow me to continue improving myself.

# Contents

|  |            |
|--|------------|
| <b>Abstract</b>  | <b>i</b>   |
| <b>Acknowledgements</b>  | <b>ii</b>  |
| <b>Contents</b>  | <b>iii</b> |
| <b>List of Figures</b>   | <b>v</b>   |
| <b>Introduction</b>  | <b>vii</b> |
| <b>1 Heterogeneous Computing</b>                                   | <b>1</b>   |
| 1.1 Motivation . . . . .   | 1          |
| 1.2 GPUs as computing units . . . . .                              | 4          |
| 1.3 Programming on GPUs . . . . .                                  | 6          |
| 1.3.1 CPU and GPU multithread comparison . . . . .                 | 8          |
| <b>2 Introduction to Domain Wall Dynamics under Nonlocal STT</b>   | <b>10</b>  |
| 2.1 Theory . . . . .   | 10         |
| 2.1.1 Spintronics . . . . .  | 10         |
| 2.1.2 Spin Transfer Torque . . . . .                               | 11         |
| 2.1.3 Domain Wall . . . . .  | 12         |
| 2.1.4 Spin Torque in Domain Walls . . . . .                        | 12         |
| 2.2 Domain Wall Dynamics under Nonlocal STT . . . . .              | 13         |
| 2.2.1 Theoretical Approaches . . . . .                             | 13         |
| 2.2.2 Experiment . . . . .   | 14         |
| 2.3 Numerical Solution . . . . .                                   | 15         |
| 2.3.1 Finite differences in the time domain . . . . .              | 15         |
| 2.3.1.1 Boundary conditions . . . . .                              | 17         |
| 2.3.2 Fourth order Runge and Kutta method . . . . .                | 19         |
| <b>3 Implementation of Domain Wall Dynamics under Nonlocal STT</b> | <b>21</b>  |
| 3.1 Simulation . . . . .   | 21         |
| 3.1.1 Data allocation and threads . . . . .                        | 22         |
| 3.1.2 Initial Calculations . . . . .                               | 25         |
| 3.1.3 Numerical Methods . . . . .                                  | 25         |
| 3.1.3.1 Finite differences in the time domain . . . . .            | 26         |
| 3.1.3.2 Zhang and Li Model . . . . .                               | 28         |

|          |   |           |
|----------|---|-----------|
| 3.1.3.3  | Runge and Kutta   | 29        |
| 3.1.4    | Calculate effective beta                                | 29        |
| 3.2      | Validation  | 30        |
| <b>4</b> | <b>Heterogeneous Performance Analysis and Practices</b> | <b>32</b> |
| 4.1      | Practices   | 32        |
| 4.2      | Performance Metrics                                     | 34        |
| 4.2.1    | Timing  | 34        |
| 4.2.2    | Bandwidth   | 34        |
| 4.3      | Memory Handling with CUDA                               | 35        |
| 4.3.1    | Global Memory   | 36        |
| 4.3.2    | Shared Memory   | 37        |
| 4.3.3    | Constant Memory   | 37        |
| 4.3.4    | Texture Memory  | 38        |
| 4.3.5    | Thread Synchronization                                  | 39        |
| 4.4      | Concurrent Kernels                                      | 39        |
| 4.5      | Kernel Analysis   | 40        |
| 4.6      | Hardware constraints                                    | 41        |
| 4.6.1    | Thread Division   | 42        |
| 4.7      | Visual Profiler   | 42        |
| 4.7.1    | Profiler Kernel Report                                  | 44        |
| 4.7.2    | Collect Data On Remote System                           | 45        |
| <b>5</b> | <b>Optimization Results</b>                             | <b>46</b> |
| 5.1      | Supercomputer “Piritakua”                               | 46        |
| 5.1.1    | Architecture Differences                                | 47        |
| 5.2      | Optimization  | 48        |
| 5.2.1    | Branching   | 50        |
| 5.2.2    | Concurrent Kernels                                      | 51        |
| 5.2.3    | Shared Memory   | 53        |
| 5.2.4    | Structure of Arrays, SAO                                | 55        |
| 5.2.5    | Occupancy   | 57        |
| 5.3      | Optimization results                                    | 57        |
| <b>6</b> | <b>Conclusions and future work</b>                      | <b>62</b> |

# List of Figures

|     |  |    |
|-----|--|----|
| 1.1 | GPU and CPU performance comparision . . . . .              | 2  |
| 1.2 | Architecture of NVIDIA's SM . . . . .                      | 4  |
| 1.3 | NVIDIA's GPU architecture . . . . .                        | 5  |
| 1.4 | Programming Cycle . . . . .                                | 6  |
| 1.5 | CUDA's 2D thread grid . . . . .                            | 8  |
| 1.6 | Memory transfer between CPU and GPU . . . . .              | 8  |
| 1.7 | CPU Core process . . . . .                                 | 8  |
| 2.1 | Electron carries spin, charge and magnetic . . . . .       | 11 |
| 2.2 | Domain Wall VW, ATW . . . . .                              | 12 |
| 2.3 | Domain Wall nanowire . . . . .                             | 13 |
| 2.4 | Asymmetric Transverse Wall results . . . . .               | 15 |
| 2.5 | Vortex Wall results . . . . .                              | 15 |
| 2.6 | FDTD grid . . . . .  | 16 |
| 2.7 | Sampled at regular intervals a, Taylor expansion . . . . . | 17 |
| 2.8 | Euler Method . . . . .                                     | 19 |
| 2.9 | Fourth order Runge and Kutta Method . . . . .              | 20 |
| 3.1 | Control flow . . . . .                                     | 23 |
| 3.2 | Grid layout . . . . .                                      | 24 |
| 3.3 | 2D Flatten array . . . . .                                 | 25 |
| 3.4 | Laplacian block calculation . . . . .                      | 27 |
| 4.1 | PCIe Bandwidth . . . . .                                   | 33 |
| 4.2 | GPU application practices . . . . .                        | 33 |
| 4.3 | Schematic cache hierarchy of a CUDA GPU . . . . .          | 36 |
| 4.4 | Different memory types . . . . .                           | 36 |
| 4.5 | Texture Memory . . . . .                                   | 38 |
| 4.6 | Concurrent Kernels . . . . .                               | 40 |
| 4.7 | Visual Profiler metrics . . . . .                          | 43 |
| 4.8 | Visual Profiler timeline and stream process . . . . .      | 44 |
| 5.1 | Initial GPU results . . . . .                              | 49 |
| 5.2 | he execution flow . . . . .                                | 50 |
| 5.3 | Initial Streams . . . . .                                  | 52 |
| 5.4 | Streams kernels Tesla K20 . . . . .                        | 53 |
| 5.5 | Waiting time in concurrent kernels . . . . .               | 53 |
| 5.6 | Shared Memory Strategy . . . . .                           | 55 |
| 5.7 | Array of structures (AOS) . . . . .                        | 56 |

|   |    |
|---|----|
| 5.8 Structure of Arrays (SAO) . . . . .               | 56 |
| 5.9 Overall simulation time . . . . .                 | 59 |
| 5.10 Speedup performance output . . . . .             | 59 |
| 5.11 Optimization results with the Profiler . . . . . | 60 |
| 5.12 Optimization speedup overview . . . . .          | 60 |

# Introduction

Commodity graphics processing units (GPUs) are becoming increasingly popular to accelerate scientific applications due to their low cost and potential for high performance when compared with central processing units (CPUs). A large number of contemporary problems and scientific research are being benefit from this new technology. There has been considerable progress in implementing the hardware and the supporting infrastructure for GPUs programming and streaming architectures. This thesis is a study of heterogenous computing using NVIDIA's GPU applied to computational physics.

The first chapter is a overview of heterogeneous architecture programming with NVIDIA's GPUs using NVIDIA's programming framework, Compute Unified Device Architecture (CUDA). The second chapter is the study of the phenomenon known as spin-diffusion on magnetic configurations at the nanoscale. Some of such configurations are known as domain walls. These magnetic configurations can be observed experimentally in NiFe soft nanostripes but they are really complicated to produce. Due to this, we use the massively parallel capabilities of a single NVIDIA GPU to numerically solve a mathematical equation, known as the Zhang-Li model. The numerical implementation is done by using NVIDIA's CUDA platform, which is explained in chapter 3. In addition, the numerical solution is a the method known as Finite Differences in the Time Domain (FDTD) whose integration is done using a 4th order Runge-Kutta integration. The fourth chapter focus on optimization techniques and practices, to gain the most performance out of the hardware capabilities. The fifth chapter are the results collected by applying optimization techniques to the initial CUDA code. Optimizations such as concurrent kernels, shared memory, branching and occupancy. The outcome is compared by launching the code on-to several GPUs nodes using the supercomputer "Piritakua". Finally, the last chapter of the thesis is a conclusion of the work and future research.

# Chapter 1

## Heterogeneous Computing

Heterogeneous computing refers a system that combines several processor types to gain more performance. Typically using a single or multi-core computer processing units (CPUs) and a graphics processing units (GPUs). Frequently GPUs are known for 3D graphics rendering, video games and video editing, but GPUs are becoming increasingly popular for accelerating computing applications and scientific research due to their low price, high performance and relatively low energy consumption per FLOPS (floating point operations per second) when compared with the CPUs. This chapter provides an overview of GPUs within the High Performance Computing (HPC) context, their advantages and disadvantages and how they can be integrated into a scientific software and research.

### 1.1 Motivation

The GPU has been an essential part of personal computers since the early 1990s. Over the course of 30 years the graphics architecture has evolved from drawing a simple 3D scene to being able to program each part of the GPU graphics pipeline. Their role became more important in the 90s with the first-person shooter video game DOOM by id Software. The demanding video game industry has brought year by year more realistic 3D graphics. Consequently new innovative hardware capabilities have been developed to increase the graphics pipeline and the render output. This led to a more sophisticated programming environment with a massive parallel capabilities.

The fixed graphics pipeline (fixed functions on the GPU) was introduced in the early 90s, allowing various customization of the rendering process. However, only allowed some modifications of the GPU output. Specific adjustments were extremely complicated

did not allow custom algorithms. In 2001 NVIDIA and ATI (AMD) introduced the first programmability to the graphics pipeline. Which could control millions pixels and vertex output in a single frame, moreover it out-performed the CPU in rendering video. In addition graphics shift from the CPU to the GPU. This was the beginning of GPU parallel capabilities [19].

At first the GPUs were only used for general-purpose computing (GPGPU) like computer graphics, but in recent years the GPU has been used to accelerate scientific research, analytics, engineering, robotics and consumer applications.

GPUs are attractive for certain type of scientific computation as they offer potential seed-up of multi-processors devices with the added advantages of being low cost, low maintenance, energy efficient, and relatively simple to program. Many algorithms in applied physics are using GPUs to improve their performance over the CPU. Some areas of scientific research that obtain the benefit of heterogeneous computing are: Molecular Dynamics, Quantum Chemistry, Computational Structural Mechanics and Computational Physics [20].

In any case, for a given simulation a compromise between speed and accuracy is always made. The current tendency of the CPU relies on increasing the clock speed, decreasing the size of transistor and finally adding more cores per unit and be able to work in a parallel manner. Therefore there are limitations to this paradigm [25].

### Power Wall

The CPUs single core has not gone beyond the 4GHz barrier, a paradigm shift from a single core to a multi-core CPUs, also the power use of CPUs is very high per Watt. The figure 1.1 shows the comparison of performance between the GPU and CPU.

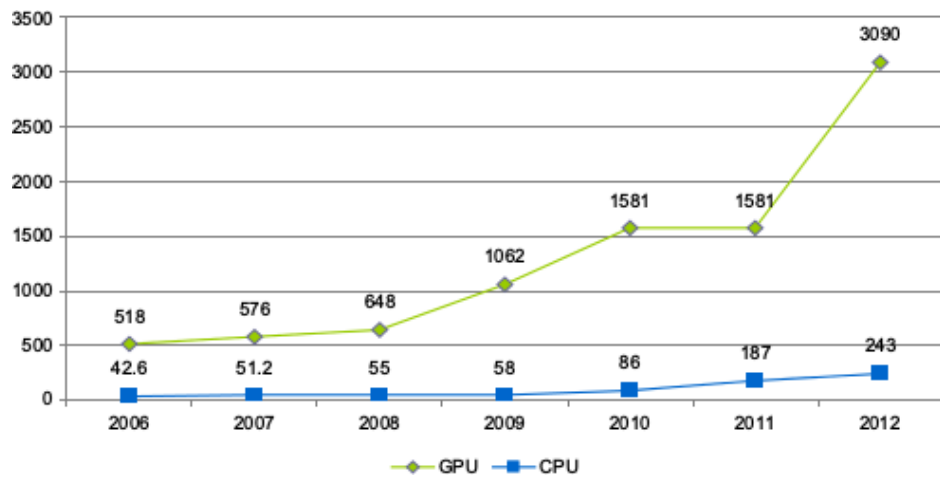


FIGURE 1.1: GPU and CPU peak performance in gigaflops

## Memory Wall

This refers to the growing disparity of speed between CPU and the memory outside the CPU chip. Some applications have become memory bound, that is to say computing time is bounded by the transfer memory between the CPU and all the hardware devices connected to the CPU, commonly to the Peripheral Component Interconnect (PCI) chip. In conclusion, the computing time is bounded by the memory and not by the time calculations performed on the CPU.

## Parallelism Wall

This indicates a law that indicates the number of parallel processes. The number  $N$  parallel processes is never ideal and always depends on the problem. The speedup is described by Amdahl's Law in terms of the fraction of parallelized work  $f$  [25].

$$\text{Speedup} \leq \frac{N}{f + N(1 - f)}$$

The current paradigm of using CPUs for computing is growth unsustainable. In 2012, Japan among the countries with elite supercomputers, builded the machine "K Computer", with 705,024 multi-core CPUs, achieving up-to 11.3 petaflops ( $10^5$  flops). Furthermore, the computer is one of the most power efficient supercomputer in the world with a total of 12.66 megawatts (MW), in other words 830 Mflops/watt. This is enough to power a small town of 10,000 homes. If the current trend of power use continues, the next supercomputer would require 200 MW of power, this would require a nuclear power reactor to run it [31]. However, in 2013 Oak Ridge Nacional Laboratory (U.S) built a supercomputer that combines CPUs and GPUs, the Titan. It obtains an astonishing 24 petaflops theoretical peak performance. Moreover, with a power consumption of 8.2 MW. They demonstrated that is possible to built a supercomputers that combines CPUs and GPUs, which enables a higher performance and lower power consumption compared to a CPU based supercomputer [23].

As said the GPU exceeds the CPU in calculations per second FLOPS with a low energy consumption. However, the GPU is designed to launch small amounts of data in parallel with only several instructions, in other words the GPU swap, switch threads very fast and they are extremely lightweight. In a typical GPU system, thousands of threads are waiting for call request to start working. While on the CPU only run up-to 24 threads on a hex-core processor. They can execute a single operation on comparatively large set of data with only one instruction. Although this can be extremely cost-wise operation on the GPU.

## 1.2 GPUs as computing units

The GPU, unlike its CPU cousin, has thousands of registers per SM (Streaming Multiprocessor), which are arithmetic processing units. An SM, in other words, is similar to a multi-thread CPU core. On a typical CPU has two, four, six or eight cores. On a GPU as many as  $n$  SM core. The SM are configured in such a way that they are able to access memory location close by. We can see this in the figure 1.2. For a particular calculation, all the stream processors within a group execute exactly the same instruction on a particular data stream, then the data is sent to the upper level, the host (CPU) [6].

CUDA cores, are the number of processors in a single NVIDIA GPU chip. For example one of the first GPU capable of running CUDA code was the NVIDIA 9800 GT, which had 112 cores, while the latest high-end GPU GTX 980 has 2048 cores.

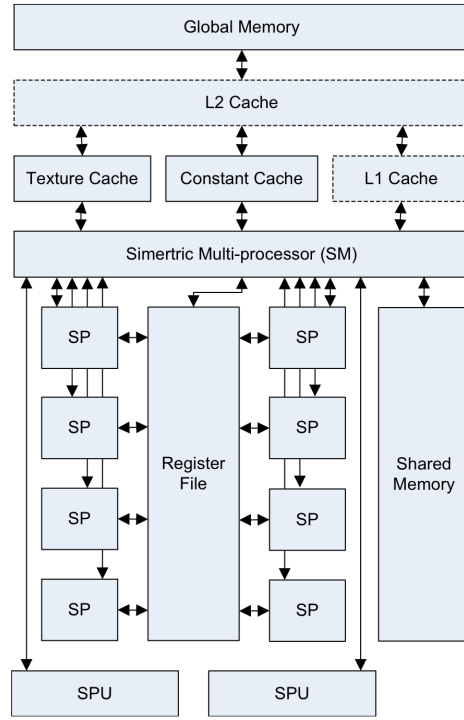


FIGURE 1.2: SM Architecture [6].

Each CUDA core can execute a sequential thread, just like a CPU thread, which NVIDIA calls it Single Instruction, Multiple Thread (SIMT). In addition, all cores in the same group execute the same instruction at the same time, much like classical SIMD (Single instruction, multiple data) processors. SIMT handles conditionals somewhat differently than SIMD, though the effect is much the same, where some cores are disabled for conditional operations, in other word a single instruction is executed throughout the device.

Being able to efficiently use a GPU for an application requires to expose the inherent data-parallelism Optimized for low-latency, serial computation. This can be seen in contrast with a CPU, which is optimized for sequential code performance, fast switching registers and sophisticated control logic allowing to run single complex programs as fast as possible, which is not possible on the GPU. Memory management is very important for GPUs. This refers how to allocate memory space and transfer data between host (CPU) and device (GPU). While the CPU memory hierarchy is almost non-existent, on the GPU inherent data is important [15]. The figure 1.3 illustrates the memory hierarchy of the device. In addition the global memory is huge in comparison with the L1/Cache and the texture memory. However, the access to the global memory is slow in comparison to the other. We can observed in the figure how the data is sent from the host to the device and vi-versa.

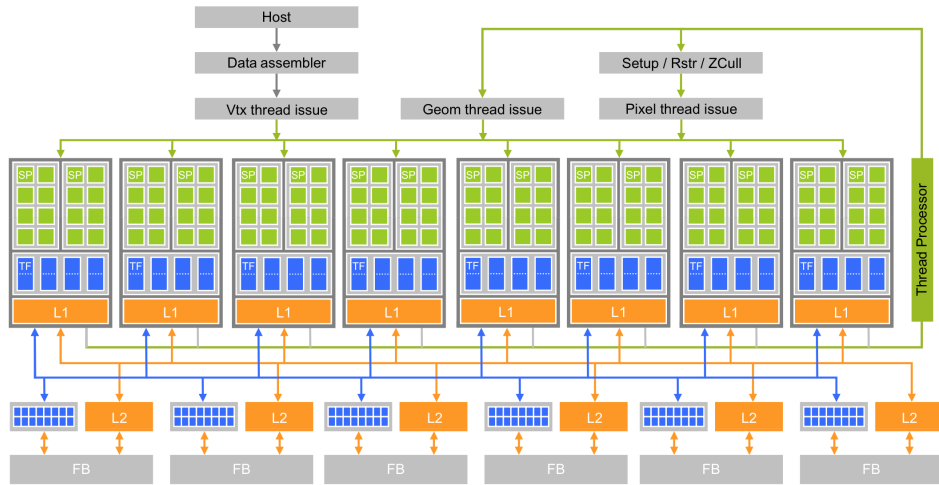


FIGURE 1.3: Unified programmable processor array of the GeForce 8800 GT graphics pipeline [15].

On the GPU, floating point precision and optimization are very important. However, there is a penalty for choosing either performance or precession. All the GPUs are optimized for single precision floating operations, a 24 bit size. NVIDIA, also provides a double precision point, size of 53 bits. Which is a standard based on IEEE 754 notation. Normally the GPU uses the single precession(SP) by default, if chosen a double precision (DP), normally there is a penalty between 2x and 4x speedup[35]. Libraries such as CUBLAS and CUFFT provides useful information how NVIDIA handles floating point operations under the hood.

### 1.3 Programming on GPUs

There exist among many, two main computing platforms, NVIDIA’s Compute Unified Device Architecture (CUDA), and Khronos’s Open Computing Language (OpenCL). NVIDIA’s CUDA provides the necessary tools, frameworks and library to program parallel application. While, the OpenCL is a open standard framework meaning that is possible to do parallel computing on other GPUs, like on AMD cards. Programmers can easily port their code to others graphics cards. However, CUDA has more robust debugging and profiling for GPGPU computing. The two frameworks are developed to be close to the hardware layer, using the C programming language as primarily programming language. Furthermore, CUDA provides both a low level API and a higher level API. Those who are familiar to OpenCL and CUDA, can easily modify their code to work on either platform [15].

CUDA programming model views the GPU as an accelerator processor which calls parallel programs throughout all the SM [36]. In addition, the CUDA parallel programs are only launched on the device (GPU) and are named as kernels. The kernels are executed across a large amount of threads, which contains the CUDA code. The basic idea of programming on a GPU is simple, the following steps explains the procedure 1.4.

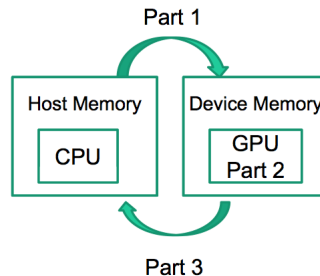


FIGURE 1.4: Programming Cycle between the CPU and GPU [29]

- Create memory(data) for the host (CPU) and devices (GPUs)
  - Send the data host memory to the highly parallel device.
  - Do something with data on the device, e.g. matrix multiplication, calculation, parallel algorithm.
  - Return the data from the device to the host.

The structure of CUDA reflects the coexistence of CPU and GPUs. The CUDA code is a mixture of both host code and device code. Moreover, the device code is an extension of the C compiler with additional namespaces/CUDA keywords for parallel code,

the CUDA compiler is called NVCC. The host code is the standard low level ANSI C language. However, is possible to program applications in C++, Python and Fortran. While the standard C code has extension marked as .c for source and .h for headers files, the CUDA code has extensions of .cu for source files and .cu.h.

Kernels are launched or executed on a large amount of threads in the SM. They can be configured by threads per block and by block per grid. The thread and block configuration is illustrated in the figure 1.5. A thread is the simplest executing process. It consists of the code of the program, the particular point where the code is being executed [15]. In addition all the threads in a kernel can access the global memory (RAM), figure 1.3 illustrates the physical position. Moreover, many threads form a block, and many blocks form a grid. CUDA handles the execution of the random-access threads, which take up-to very few clock cycles in comparison to CPU threads.

Each of the threads can be access by a implicit variable that identifies its position within the thread block and its grid. The thread access for the x coordinate is showed in the code 1.1. This is only the case for 1D block, which is widely used for shared memory access (see chapter 4) [29].

---

```
int index = blockIdx.x * blockDim.x + threadIdx.x;
```

---

LISTING 1.1: 1D thread block operation on a CUDA kernel

For the case of a 2D thread block, the code 1.2 describe such configuration. In addition, the 2d thread block is the most common thread block configuration. Is also possible to configure a 3D thread block just by adding the z coordinate to the threadIdx index. However, is very limited.

---

```
int i = blockIdx.x * blockDim.x + threadIdx.x;
int j = blockIdx.y * blockDim.y + threadIdx.y;

int index = j * YSIZE + i;
```

---

LISTING 1.2: 2D thread block operation on a CUDA kernel

$$\text{blockIdx.x} \times \text{blockDim.x} + \text{threadIdx.x}$$

In CUDA, host memory and device memory have separate memory spaces. Both of them have physically a separated location, for example, the RAM for either the CPU o the GPU. Furthermore, the programmer requires to send data from the host memory to the device's global memory (RAM) and vice-versa. The process is illustrated in figure 1.3. Memory which is allocated in the device needs to be freed on the device, the same occurs for the host memory. Moreover, the process is accomplish with similar devices

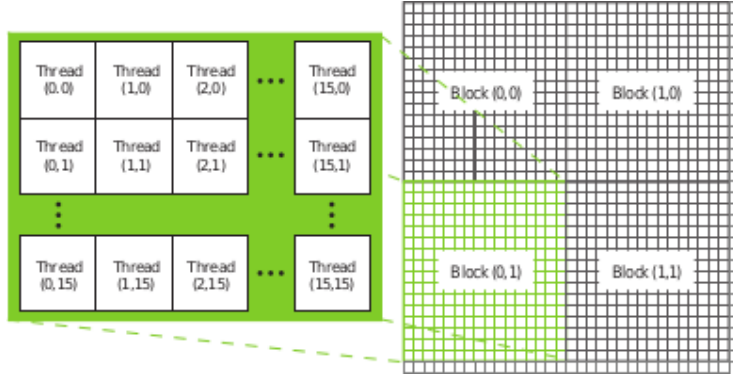


FIGURE 1.5: Thread per block division and block per grid [15].

operations, free or delete in C/C++. Some of the operations are performed by CUDA's Application Programming Interface (API) on behalf of the programmer [15].

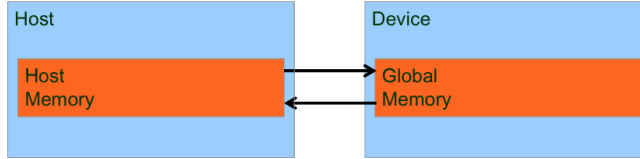


FIGURE 1.6: Memory transfer between CPU and GPU [15]

### 1.3.1 CPU and GPU multithread comparison

Current CPUs are typically multicore systems, which are capable of parallelizing code fairly easily. In addition suggest a parallel system. However, we would require a large infrastructure [29]. For example, if we want to implement a simple vector addition using the CPU cores, we would require to compute a portion of the code on each core, one core the evens and the other core the odds, see figure 1.7. Furthermore, this makes the implementation difficult to scale and require many cores, which are not so easily available after a 8 core system.

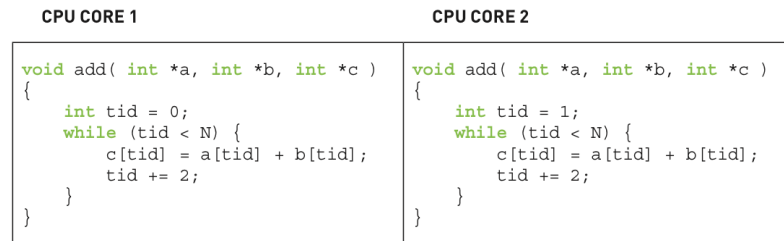


FIGURE 1.7: CPU Core process [15].

On the GPU we are able to accomplish the same result of the CPU with least amount of code. The code 1.3 demonstrate how to evaluate an addition of two matrices.  $a$  and

*b*, then return the result in the matrix *c*. The difference between the codes, is that the GPU executes the kernel across all threads configured by the kernel call. Moreover, enables a highly parallel process with just a couple lines of code.

---

```
--global__ void add( int *a, int *b, int *c ) {
    int tid = blockIdx.x;
    if (tid < N)
        c[tid] = a[tid] + b[tid];
}
```

---

LISTING 1.3: GPU Kernel threads launch

For example, to execute a kernel with  $32 \times 32$  threads per block and  $15 \times 4$  blocks per grid, we just include the block and the threads dimensions when calling the kernel in the main loop 1.4. Finally, the kernel will spam the CUDA code across all the configured threads in the device.

---

```
dim3 blocks(15, 4);
dim3 threads(32, 32);
add<<< blocks2, threads, 0 >>>(A, B, C);
```

---

LISTING 1.4: Kernel call with configurable threads per block and block per grid

To conclude, this chapter provided a overview of heterogeneous programming in a modern context. CUDA enhance the C language with parallel computing support. In addition, is possible to launch enormous amounts of parallel threads, opposite of few threads on the CPU. The number of GPU cores will continue to increase in proportion to increase in available transistors as silicon process improve. In addition, GPUs will continue to go through vigorous architectural evolution. Despite their demonstration high performance on data-parallel applications.

## Chapter 2

# Introduction to Domain Wall Dynamics under Nonlocal STT

This chapter is a brief overview of the theory of spintronics and the study of Domain Wall Dynamics under Nonlocal Spin-Transfer-Torque. Which quantitatively test the effects of spin-diffusion, on real Domain Wall (DW) structures, by numerically implementing the Zhang-Li model on a NiFe soft nanostrip. The numerical method used for the solution is a the method known as Finite Differences in the Time Domain (FDTD) on a 3d cell grid with whose integration is done using a 4th order Runge-Kutta integration (RK4).

### 2.1 Theory

The electrons not only carry an elementary unit of charge  $e$ , but also carries an elementary unit of angular momentum. Whenever we produce an electrical current by inducing motions of electrons, it could indeed be viewed as a collection of little magnets that are moving around (see Figure 2.1). In other words, any electron charge transport is simultaneously accompanied by a transport of spin, or magnetic moment carried by these electrons [34].

#### 2.1.1 Spintronics

Spintronics is a new type of electronics that exploits the spin degree of freedom of an electron in addition to its charge [37], figure 2.1. The interest is motivated by the quest to understand basic physical principles underlying the electron and spin interactions in materials and possible technological applications. The field of spintronics has attracted

massive interest since the discovery of giant magnetoresistance (GMR) effect in 1988 by Albert Fert and Peter Grünberg who were awarded the 2007 Nobel Prize in physics. The GMR effect has been widely used in hard disk drives (HDD), which have delivered a huge impact on industries and consumer electronics. Spintronics is a promising technology which will complement the present electronics with additional "spin" quantum freedom to charge freedom that is currently used in devices [11].

### 2.1.2 Spin Transfer Torque

A torque is simply a time rate of change of angular momentum [1]. Hence, spin transfer torque (SST) occurs when spins flowing from one layer to another can reorient the magnetization in the layers, see figure 2.3. The magnetization of the ferromagnet changes the flow of spin angular momentum by exerting a torque on the flowing spins to reorient them, and therefore the flowing electrons must exert an equal and opposite torque on the ferromagnet. This torque that is applied by non-equilibrium conduction electrons onto a ferromagnet is what we will call the spin transfer torque [1].

Spin current which is a flow of spin angular momentum, is generated in addition to the charge current. The spin current normally appears in ferromagnets. However, it should be able to be generated in non-magnets. The simplest method of generating a spin-polarized current in a metal is to pass the current throughout a ferromagnetic material. A common application is the GMR as mentioned before [32].

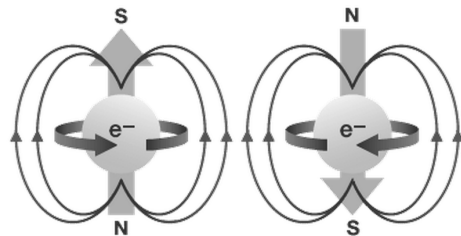


FIGURE 2.1: Electrons not only carries charge, but also spin and magnetic properties [13].

Spin polarized transport occurs naturally in any materials which have a spin imbalance between spin-up and spin-down at the Fermi Level. It occurs at spin-down electrons as nearly identical, but states are shifted in energy with respect to each other. The Fermi level is the highest energy level which an electron can occupy at the absolute zero temperature. Since at absolute zero temperature the electrons are all in the lowest energy state hence the Fermi level is in between the valence band and the conduction band [32].

### 2.1.3 Domain Wall

An abrupt in magnetization at the boundary of two anti-aligned domains is not a favorable condition. Domain walls form between such domains as means of minimizing the energy of the two anti-aligned domains. Domains walls are transitions layers in which the magnetization changes gradually from one magnetization to another. In other words the boundaries between regions of uniform magnetization. The gradual change prevents the large increase in exchange energy that would accompany an abrupt change in the magnetization angle. Common domain wall geometric include Bloch walls, Néel walls and vortex walls [9]. In this study only two DW are analyzed the Vortex Wall and the Asymmetric Transverse Wall.

#### Vortex Wall (VW)

In the case of Vortex wall the magnetization rotates in the plane perpendicular to the domain wall, but the local magnetization is wrapped around a single vortex point, see figure 2.2.

#### Asymmetric Transverse Wall (ATW)

The transverse wall has a reflection symmetry about a line perpendicular to the strip axis, and a lack of symmetry about the center line of the strip. However, asymmetric transverse wall, is the absence of that symmetry, see figure 2.2.



FIGURE 2.2: Vortex Wall (VW) and Asymmetric Transverse Wall (ATW) [5].

### 2.1.4 Spin Torque in Domain Walls

Domain walls are the basis for various spintronics devices that uses magnetic momentums, in other words spin of electronics, the used of the spin degree of freedom. The figure 2.3 illustrates a micromagnetic model of the domain wall trapped in a nanowire. The domain wall can be pushed along the wire in a controllable manner by applying an external magnetic field or by passing an electrical current through the wire [14].

The energy of the incoming carrier is no the only factor that determines whether or not it passes to the other side of domain wall, the spin also must be taken into account. Since each spin orientation experiences a different potential. Simulation of such properties is necessary.

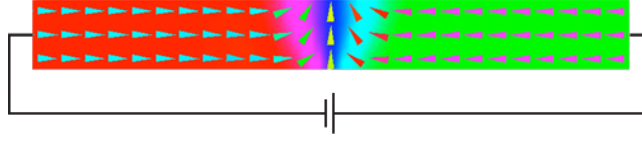


FIGURE 2.3: Domain Wall in a nanowire while passing a current

Spin Torque induced domain wall motion opens up a host of possibilities for applications. The success of spintronics untimely depends on our ability to precisely control the polarization of electrons transported within the actual thin film structure [27]. Advances in spintronics recognized by 2007 Nobel Prize in Physics have enabled over the last decade advances in computer memory, in hard drives, this is a metal based structures which utilize magnetoresistive effects to save and read data from a magnetic disk [32]. An interesting application using this idea is new design for a different type memory disk drive called racetrack memory by Parkin in 2008[24]. The racetrack memory stores bits along a single ferromagnetic wire. To write and read information, a current is applied along the wire that moves the bits to writing or reading unit.

## 2.2 Domain Wall Dynamics under Nonlocal STT

The motion of domain walls due to spin transfer torque (STT) of electrons has been studied theoretically and experimentally. Furthermore, moving magnetic domain walls using electric currents via spin-torque effects, is one the recent developing in spintronics. We analyze a moving domain wall on a soft nanostrip, because it concentrates all of the magnetization non-uniformity, which acts as a built-in detector for spin torques. The inclusion of STT into micromagnetics has up to now been performed with local terms that express the STT as a function of only the local magnetization [5].

### 2.2.1 Theoretical Approaches

The inclusion of STT into micromagnetics has up to now been performed with local terms that express the STT as a function of the local magnetization only. The magnetization dynamics is described by the classical Landau-Lifshitz-Gilbert (LLG) equation [5], expanded with a STT variable 2.1.

$$\frac{\partial \vec{m}}{\partial t} = \gamma_0 \vec{H}_{eff} \times \vec{m} + \alpha \vec{m} \times \frac{\partial \vec{m}}{\partial t} - \vec{T} \quad (2.1)$$

This novel idea of incorporating spin torque into the LLG equation has itself been incorporated into a model proposed by Zhang-Li in 2004 [18]. The LLG equation 2.1 is incorporated effects of a spin-polarized current in a magnetic system, and the resulting spin transfer. They develop a form for the spin torque based on the spatial variation of the magnetization, as especially appropriate approach for domain walls. Then in 2005 the same authors Zhang-Li extended this idea working out the difference between the adiabatic and non-adiabatic torque contributions. Which lead to an even longer magnetization dynamics equation [38] [9].

$$\frac{\partial \delta \vec{m}}{\partial t} = D_0 \nabla^2 \delta \vec{m} - \frac{1}{\tau_{sd}} \delta \vec{m} \times \vec{M} - \frac{1}{\tau_{sf}} \delta \vec{m} + (\vec{\mu} \cdot \vec{\nabla}) \vec{M} \quad (2.2)$$

The equation 2.2 is referred to Zhang-Li model, represents a non-adiabatic spin torque, with the presence of spin diffusion. Spin diffusion is a process by which magnetization is exchanged spontaneously between spin, which spin is able to accumulate in metals. The associated diffusion current flows in all directions, giving rise to nonlocal effects. The diffusion term of the equation 2.2 which carriers drift-diffusion equation implies that the spin density does not depend solely on the local magnetization, which gives rise of nonlocal magnetics effects [5].

Amongst the rapidly growing variety of proposed and developed spin structures, nonlocal spin detection devices, where measurement and current excitation paths are spatially separated, have recently gained a prominent position [37].

### 2.2.2 Experiment

We Quantitatively test the effects of spin diffusion, on real Domain walls structures, this is done by numerically solve the Zhang-Li model into micro-magnetics, using the equation 2.2. Zhang-Li research [38] initially solves analytically the diffusion equation 2.2, However, ignoring the term of spin diffusion. In this numerically simulation we solve such equation using the spin diffusion term.

The sample considered is a 300 nm wide and 5 nm tick NiFe soft nanostrip. This dimensions are widely used for experimental use. Two Domain walls are used a Asymmetric Transverse Wall (ATW) and a Vortex Wall (VW). ATW maps of magnetization components of non equilibrium spin accumulation under a uniform current density with  $D = 0, 1$  and  $10 \text{ nm}^2/\text{ps}$ . See figure 2.4.



FIGURE 2.4: Asymmetric Transverse Wall (ATW) results [5].

Vortex Wall (VW) same as for ATW, we point out the noticeable effect of the diffusion constant around the vortex core, which is the smallest feature of the wall. See figure 2.5.

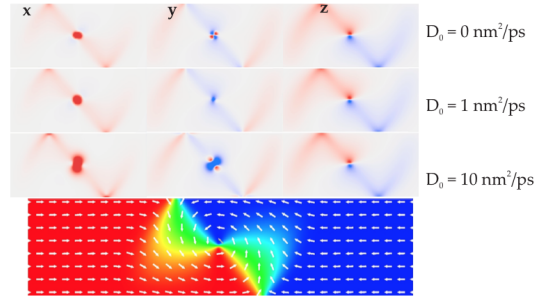


FIGURE 2.5: Vortex Wall results [5].

## 2.3 Numerical Solution

The equation 2.2 is physically realistic, However, computationally expensive. Therefore we numerical methods to solve such equation. The numerical methods used for the solution is a the method known as Finite Differences in the Time Domain (FDTD) whose integration is done using a 4th order Runge-Kutta integration.

### 2.3.1 Finite differences in the time domain

The finite difference in the time domain (FDTD) method is able to solve complicated problems. However, it is generally computationally expensive. Solutions may require a large amount of memory and computation time [30]. FDTD is a numerical analysis technique use for approximating solutions to the associates system of differential equations. The method belongs in the general class of grid-based differential numerical modeling methods. Please read reference [7] for more information about the demonstration of such numerical methods for this section.

The FDTD method essentially uses a weighted summation of functions values at neighboring points to approximate the derivate at a particular point, in this case a point in a 3d grid. The result for each cell is based on the results from the cell and its neighbors at the previous time-frame, figure 2.6.

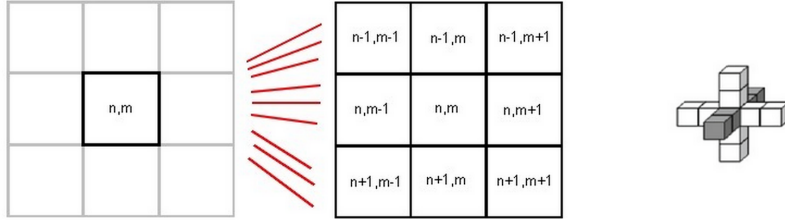


FIGURE 2.6: The result for each cell is based on evaluating the derivate cell neighbors [7].

The magnetization is sampled on a uniform rectangle mesh at points  $(x_0 + i\nabla_x, y_0 + j\nabla_y, z_0 + k\nabla_z)$ . The computational cell is centered about the sample point with dimensions.  $\nabla_x \times \nabla_y \times \nabla_z$  [7].

Looking at the equation 2.2, we need a method to calculate the first and second derivate. With the Taylor expansion we are able to perform such calculation. The Second order Taylor expansion readily yields expressions for the first and seconds central derivates. First and second-order derivates of the magnetization components in order to define the divergence of the magnetization ( $\nabla \cdot m$ ), and the components of the exchange field ( $\nabla^2 m$ ), respectively. The magnetization components along boundaries also need to be evaluated in order to define surface charges ( $m \cdot n$ ). Boundary conditions need to be incorporated in the evaluated of the effective field without loss of accuracy.

Consider a regular, differentiable one-dimension scalar function  $f(x)$  sampled at regular intervals,  $a$ , see figure 2.7. Second order Taylor expansion readily tiles expressions for the first and seconds central derivates that are widely used in numerics, namely  $\frac{df}{dx} = \frac{f_{i+1}-f_{i-1}}{2a}$  and  $\frac{d^2f}{dx^2} = \frac{f_{i+1}-2f_i+f_{i-1}}{a^2}$  [7].

However, the numerical derivation of the structure of a simple Bloch wall using such expressions soon reveals that second order Taylor expansion ledes to restricted accuracy. Fourth order expansion as actually been found to prove much superior [7].

Taylor expansion of the function  $f(x)$  around  $x = x_i$  yields where  $f^{(k)}(x_i) = f(x)$  if  $k = 0$

$$f(x) = \sum_{k=0}^{\infty} \frac{(x - x_i)^k}{k!} f^{(k)}(x_i) = \sum_{k=0}^{\infty} \frac{(x - x_i)^k}{k!} f^{(k)}$$

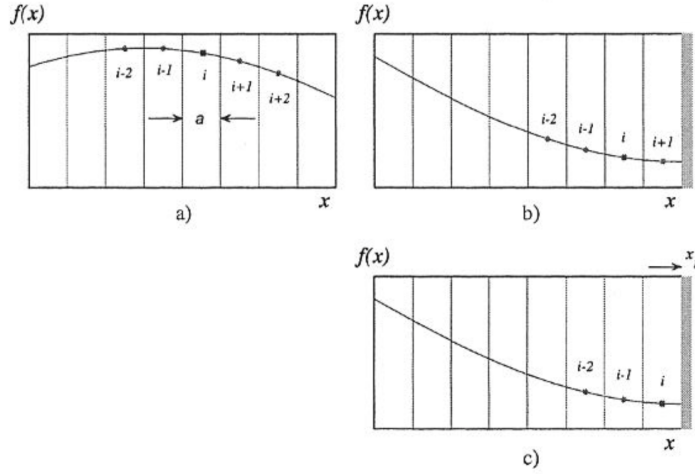


FIGURE 2.7: Sampled at regular intervals a, (a) Function of inside the grid. (b) Mesh points second to closest to boundary. (c) Mesh points closet to boundary

Applying the previous equation to nearest and next nearest neighbor to grid point  $i$  and truncation the the 4th order yields a set of four equations

The set of linear equations provide numerical estimates for the first, second, third and fourth derivatives of  $f$  at any given point  $i$ . The general form of the first and second derivate based on second nearest neighbors expansion reads:

$$f_i^{(1)} = \frac{f_{i-2} - 8f_{i-1} + 8f_{i+1} - f_{i+2}}{12a} \quad (2.3)$$

$$f_i^{(2)} = \frac{f_{i-2} + 16f_{i-1} - 30f_i + 16f_{i+1} - f_{i+2}}{12a^2} \quad (2.4)$$

The equation 2.3 for the second derivate based on second nearest neighbors expansion solves for the laplacian operator in the Zhang -Li Model equation 2.2. However, points close to the edges need to be evaluated for great precession.

### 2.3.1.1 Boundary conditions

Expressions such as 2.3 are valid when the grid point becomes closet or next-to-closest to the boundary of the magnetic box. Specific accuracy preserving, expansion need to be worked out. The general principal in the present approach is to replace equations that are missing because of the lack of grid points outside the magnetic volume by equations including explicit reference to boundary conditions [7].

Consider first a point second to closet to bound, 2.7-b. Grid point  $i + 1$  is missing for this particular geometry. However, defining  $x_R$  as the right boundary coordinate along

the  $x$  axis. The  $f^{(1)}(x_R)$  to be know along the boundary to be replace by the derivate of Taylor's expansion [7].

$$f^{(1)}(x) = \sum_{k=0}^{\infty} \frac{(x - x_i)^{k-1}}{(k-1)!} f^{(k)}(x_i) \quad (2.5)$$

Using 2.7-b.  $x_R - x_i = 3a/2$  becomes [7].

$$\begin{bmatrix} -2a & \frac{(-2a)^2}{2!} & \frac{-(2a)^3}{3!} & \frac{(-2a)^4}{4!} \\ -a & \frac{(-a)^2}{2!} & \frac{(-a)^3}{3!} & \frac{(-a)^4}{4!} \\ a & \frac{(a)^2}{2!} & \frac{(a)^3}{3!} & \frac{(a)^4}{4!} \\ 2a & \frac{(2a)^2}{2!} & \frac{(2a)^3}{3!} & \frac{(2a)^4}{4!} \end{bmatrix} \begin{bmatrix} f_i^{(1)} \\ f_i^{(2)} \\ f_i^{(3)} \\ f_i^{(4)} \end{bmatrix} = \begin{bmatrix} f_{i-2} - f_i \\ f_{i-1} - f_i \\ f_{i+1} - f_i \\ f^{(1)}(x_R) \end{bmatrix} \quad (2.6)$$

Similarly, for a point closet to boundary, reference 2.7-c, grid points  $i + 1$  and  $i + 2$  are missing. The two first equation of ... need now to be replaced by a single equation, whilst the two remaining equations need to be truncated to the third order. For the geometry illustrated in 2.7-c, the minimal set of equations now reads [7].

$$\begin{bmatrix} -2a & \frac{(-2a)^2}{2!} & \frac{-(2a)^3}{3!} \\ -a & \frac{(-a)^2}{2!} & \frac{(-a)^3}{3!} \\ 1 & \frac{(+a)}{2} & \frac{(+a/2)^3}{2!} \end{bmatrix} \begin{bmatrix} f_i^{(1)} \\ f_i^{(2)} \\ f_i^{(3)} \end{bmatrix} = \begin{bmatrix} f_{i-2} - f_i \\ f_{i-1} - f_i \\ f^{(1)}(x_R) \end{bmatrix} \quad (2.7)$$

In both cases, and second derivatives and fully determined provided  $f^{(1)}(x_R)$  be known along the boundary. For further reference please read[7]. For implementation of the laplacian boundaries conditions please read Chapter 3.

The main advantages of the finite difference approach is easy to implement, simplicity of meshing, efficient evaluation of the magnetization energy, and the accessibility of higher order methods. The main disadvantage of this approach is the sampling curved boundaries with a rectangular mesh, resulting in some what discrete approximation. In addition, it could produce a significant error in the evaluation.

### 2.3.2 Fourth order Runge and Kutta method

Modern numerical algorithms for the solution of ordinary differential equations are based on the method of the Taylor series. Algorithm such as the Runge-Kutta method are constructed so they give an expression depending of the parameter ( $h$ ), in other words the step as an approximate solution of the first terms of the Taylor series. The method is able to accurately solve a wide range of problems, but it is generally computationally expensive. Solutions require large amount of memory and computational time [26].

There exist several other computational numeric methods to solver such equations, methods such as the Euler integrator, the Midpoint Method and the Runge-Kutta fourth order (RK4) integrator method can solve differential equations. However, they differ in the numerically approximation and computation time. The RK4 is used for this simulation because its numerically more accurate when compared to the others methods.

The RK4 method differs widely from the Euler method and the Midpoint method. The Euler method is the simplest, the derivative at the starting point of each interval is extrapolated to find the next function value, see figure 2.8. Euler method only has first order accuracy while the RK4 its fourth order integrator [26].

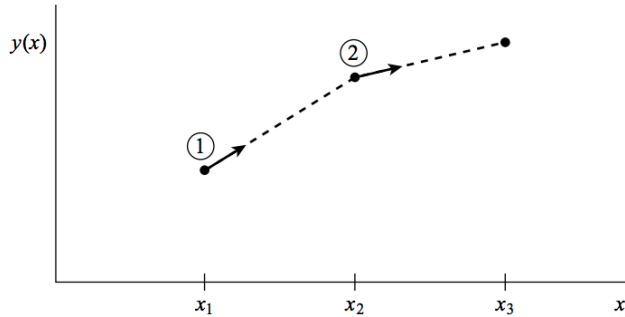


FIGURE 2.8: Euler Method, Is the simplest approximate to solver differential equation or numerically solve equations.

RK4 goes as follows:

$$y_{n+1} = y_n + 1/6K_1 + 1/3K_2 + 1/3K_3 + 1/6K_4 \quad (2.8)$$

where

$$\begin{aligned} K_1 &= h\dot{f}(x_n, y_n) \\ K_2 &= h\dot{f}(x_n + h/2, y_n + k_1/2) \\ K_3 &= h\dot{f}(x_n + h/2, y_n + k_2/2) \\ K_4 &= h\dot{f}(x_n + h, y_n + k_3) \end{aligned} \quad (2.9)$$

As the equations shows, each step, the derivative is evaluated four times, once at the initial point, twice at trial midpoints, and once at a trial endpoint. From these four values, the final value is calculated, just like the equation 2.8.

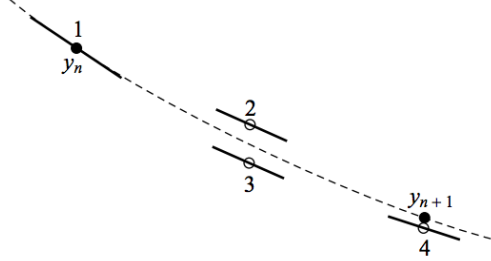


FIGURE 2.9: Fourth order Runge and Kutta method, each step the derivative is evaluated four times.

In conclusion, the simultaneous solution of the diffusive Zhang and Li model 2.2 has uncovered a qualitatively new feature of the spin-transfer torque effect in the presence of spin diffusion. Namely the dependence of the steady-state DW velocity on DW structure [5]. In summarize, we quantitatively test the effects of spin diffusion, on real Domain walls structures for ATW and VW. This is done by numerically solve the Zhang-Li model into micro-magnetics. The numerical methods used to solve such model as mentioned is the FDTD on a 3D cell grid with whose integration is done using RK4.

## Chapter 3

# Implementation of Domain Wall Dynamics under Nonlocal STT

The following chapter is the study of the heterogenous computing implementation of the Domain Wall Dynamics under Nonlocal Spin-Transfer Torque. We use the massively parallel capabilities of a single GPU to numerically solve a mathematical equation, known as the Zhang-Li model. The numerical method used for the solution is the method known as Finite Differences in the Time Domain (FDTD) whose integration is done using the 4th order Runge-Kutta. The integration is done on a 3D grid space which outputs the magnetization data of the Vortex Wall, Asymmetric Transverse Wall and a single value, the effective beta.

### 3.1 Simulation

The simulation consist in integrating the Zhang-Li model 2.2 using the 4th order integrator Runge-Kutta, which is done for a 3D grid space of 57,600 cells. The sample considered is a 300nm wide in y direction and 5nm thick in z direction. Furthermore, the sample is a soft nanostrip composed of NiFe (nickeliron alloy), a material and size widely used in experiments with this characteristics. Using this size the asymmetric transverse wall 2.4, and the vortex wall. have nearly equal energies. The numerical mesh size is  $3 \times 3 \times 5 \text{ nm}^3$ , and the calculation box has a length (x direction) of 1,200 or 3,172 nm. The table 3.1 illustrates mesh information and calculation box for the simulation [5]. In addition, the table 3.2 shows the constant values for the numerical solution of the equation 2.2 such as  $\mu$ ,  $D_0$ ,  $\tau_{sd}$  and  $\tau_{sf}$ .

| Mesh size | value | calculation box | value  |
|-----------|-------|-----------------|--------|
| Cell NX   | 480   | Box TX          | 1200.0 |
| Cell NY   | 120   | Box TY          | 300.0  |
| Cell NZ   | 1     | Box TZ          | 5.0    |

TABLE 3.1: Mesh size and calculation box

The simulation is divided into two calculations parts, the host code and the device code. The figure 3.1 illustrates the data flow for the host and the device. Each step of the simulation is going to explain in the following section with more detail. First the initial values are read from a data file, which are the initial magnetization data coordinates. Then the data set is used to calculate the initial magnetization matrices for the simulation, the initial matrices are only calculated once. Afterwards, the simulation begins with the RK4 integration, which numerically solves the Zhang-Li model 2.2. The simulation is configured to integrate 50,000 times the Zhang-Li Model before calculating the final effective Beta value. The simulation stops if the effective beta or convergence to 1.0e-9. The figure 3.1 shows the control flow of the simulation. But also illustrates the workload on the host and the device. As we can see the heavy computation operations are done on the GPU side. While on the CPU only minor intense computation are done such as I/O data, memory allocation and final beta variation. Finally 1 is the pseudo-code of the RK4 integration.

| Diffusion parameters | Value                           | Runge - Kutta 4th | Value        |
|----------------------|---------------------------------|-------------------|--------------|
| $\mu$                | 1                               | time step (dt)    | $25.0e^{-6}$ |
| $D_0$                | $1.0e^3$ nm mm <sup>2</sup> /ns | tmax              | 1.0          |
| $\tau_{sd}$          | $1.0e^{-3}$ ns                  | beta difference   | $1.0e^{-9}$  |
| $\tau_{sf}$          | $25.0e^{-3}$ ns                 | Iterations        | 50,000       |

TABLE 3.2: Diffusion parameters and Runge-Kutta 4th

### 3.1.1 Data allocation and threads

First section of the implementation begins by allocation data into several matrices for both host memory and device memory. The initial magnetization data can be either self generated by the application or by reading a file which contains information related to the magnetization. In both cases the data is divide into two blocks of data. Both blocks have 57600 (480 x 120) rows of information. The first 57600 rows contains initial magnetization x, y coordinates. The next block of 57600 rows is the initial magnetization in x, y, and z. The data being read is stored on a three temporary 2D matrix, that corresponds to the x, y, and z coordinate. In addition the three matrices are flatten into three continuous memory blocks, as showed in figure 3.3. The device code 3.1 flattens the 2d index into a single linear 1D index.

---

```

int i = blockIdx.x * blockDim.x + threadIdx.x + 2;
int j = blockIdx.y * blockDim.y + threadIdx.y;
// map the two 2D indices to a single linear, 1D index
int index = j * grid_width + i;

```

---

LISTING 3.1: Kernel Flatten from a 2 value index to a single value index.

To ensure optimal memory allocation on the GPU side is best to assign square matrices to the device. Using square memory sizes the GPU allocates efficiently the memory into the SMs and threads. The calculation for this operation is done by using the first two operations in the code 3.2.

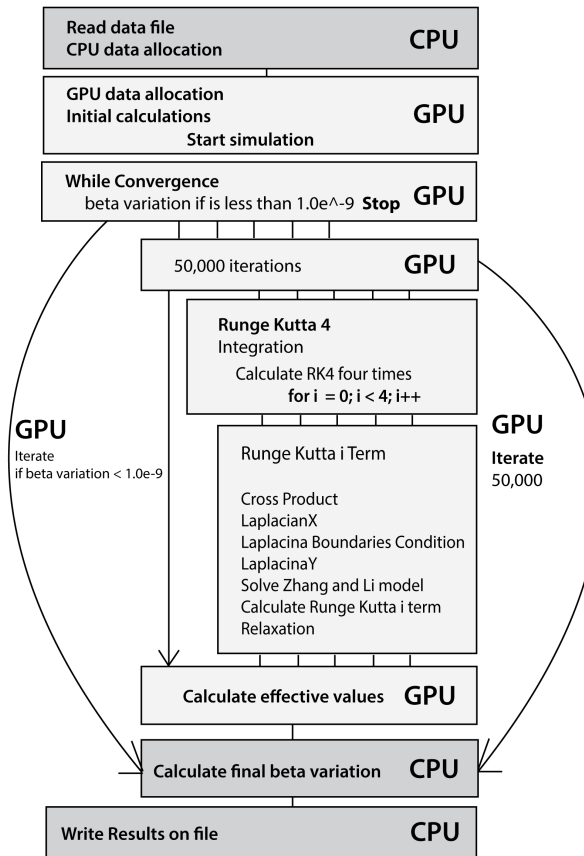


FIGURE 3.1: Control flow of the simulation for the CPU and GPU.

|               |     |                     |     |
|---------------|-----|---------------------|-----|
| Matrix size X | 480 | Device allocation X | 512 |
| Matrix size Y | 120 | Device allocation Y | 128 |

TABLE 3.3: Matrix allocation size

The magnetization data is stored on three matrices x, y, and z, each one of them with a capacity of 56,700 values, in other words 480 times 120. Base on this information we want to calculate the optimal number of grids that will ensure a complete use of the

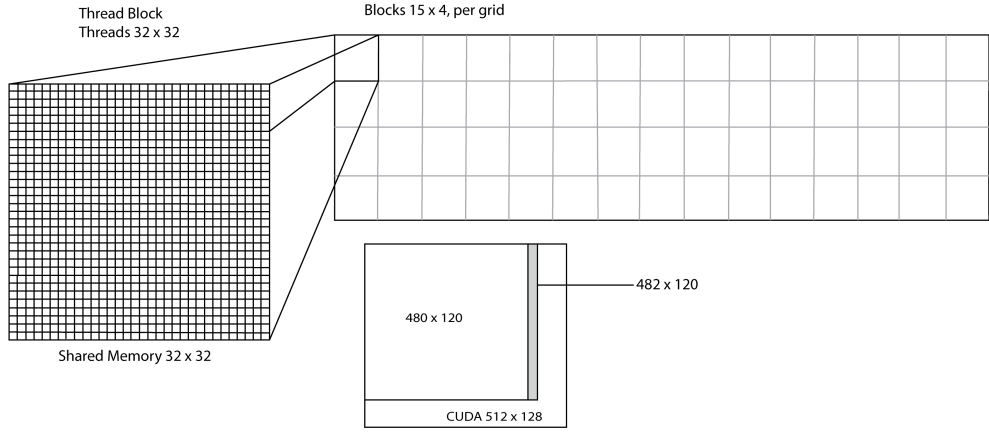


FIGURE 3.2: Memory allocation in terms of the blocks per threads and grids.

hardware resources. The number of blocks per grid corresponds dividing the dimensions of the array by the number of threads. The last two operations in 3.2.

---

```

NXCUDA = (int)powf(2,ceilf(logf(NX)/logf(2)));
NYCUDA = (int)powf(2,ceilf(logf(NY)/logf(2)));

//Setup optimum number of blocks
XBLOCKS_PERGRID = (int)ceil((float)NX/(float)XTHREADS_PERBLOCK);
YBLOCKS_PERGRID = (int)ceil((float)NY/(float)YTHREADS_PERBLOCK);

```

---

LISTING 3.2: Device capacity calculation and number of block per grid

Depending on the hardware properties, each GPU can allocate different number of threads per block and as well as a different shared memory sizes. More information about the optimal number of threads per block read the final chapter 5. The Shared memory in this implementation relies on the number of threads per block. In addition, the number of blocks depends on the input matrix and the number of threads. Examine figure 3.2.

|                     | Fermin  | Kepler  |
|---------------------|---------|---------|
| Threads per block X | 16      | 32      |
| Threads per block Y | 16      | 32      |
| Number of blocks X  | 30      | 15      |
| Number of blocks Y  | 8       | 4       |
| Shared memory       | 16 * 16 | 32 * 32 |

TABLE 3.4: Threads, blocks size

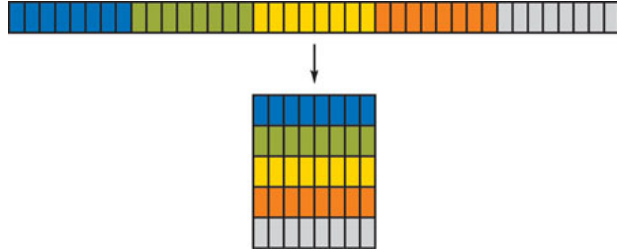


FIGURE 3.3: Converting 2D array to a single continuous block of memory

### 3.1.2 Initial Calculations

The initial step the  $\delta\vec{m}$  term is calculated from the equation 2.2 (chapter 3). this is the non-equilibrium spin density [5] domain wall at rest. The Following equations evaluates the first steps of the magnetization data3.3.

---

```
//Compute x, y and z component of source term
gsource << <blocks, threads >> >(...);
gsource << <blocks, threads >> >(...);
gsource << <blocks, threads >> >(...);

//Project source term on magnetization components by computing
//a cross product twice
gm_x_source << <blocks, threads >> >(...);
gm_x_source << <blocks, threads >> >(...);
```

---

LISTING 3.3: Initial calculations

The kernel *gsource* from 3.3 are evaluated only once, resulting with the matrix *sm*, which is used to compute the Zhang-Li model in the RK4 integration.

As mention before the matrices for CUDA are square matrices 512 x 128, however the data set is 480 x 120. Because of the matrices size difference we need to limit the number of threads execution of the CUDA kernels. To limit such threads branching with a simple if within the kernels solves this issue 3.4. Due to the boundaries condition of the FDTD a small shift of 2 indices in the x direction is necessary.

---

```
if (i > 1 && i < NX + 2 && j >= 0 && j < NY){
    //calculations
}
```

---

LISTING 3.4: Laplacian X using global memory

### 3.1.3 Numerical Methods

The following steps is where all the computational intense operations are performed. The algorithm 1 demonstrates the operations necessary for RK4 integration process. In

addition, the operations are evaluated once per iteration, composed by four time steps of the RK4, furthermore, solving the Zhang-Li model using FDTD. The algorithm exists when  $b_{eff}$  reaches an numeric error of  $1.0e^{-9}$ .

```

Data: deltam, sfrelax, sdex, sm, laplacian
Result: deltam
data initialization;
while  $b_{eff} < 1.0e^{-9}$  do
    Runge and Kutta 4th;
    for  $i = 1; i \leq 4; i+ = 1$  do
        sdex  $\leftarrow$  crossProduct(deltam, mag); calculate cross product
        FDTD with boundary condition
        laplacian  $\leftarrow$  laplacianXYBoundary(deltam);
        evaluate Zhang-Li model
        zhangLi  $\leftarrow$  solveZhang(sfrelax, sdex, laplacian, sm);
        RK4 evaluation
        rkterm(i)  $\leftarrow$  rktime(i, solveZhangLi, dt);
        if  $i == 4$  then
            | deltam  $\leftarrow$  rk4(zhangLi, tmp, dt, rkterm(1),rkterm(2), rkterm(3),rkterm(4))
        else
            | deltam  $\leftarrow$  rk4(zhangLi, tmp, dt)
        end
        evaluate RK4 term
        deltam  $\leftarrow$  rk4(zhangLi, tmp, dt)
        sfrelax  $\leftarrow$  relaxation(deltam, tau)
        if  $i == 4$  then
            | tmp  $\leftarrow$  copy(rkterm(4));
        end
    end
     $b_{eff} = \text{calculate}(\text{temp}, \beta)$ ;
end
```

**Algorithm 1:** Runge and Kutta 4th integration implementation

### 3.1.3.1 Finite differences in the time domain

The finite differences method requires the domain of interest to be broken down into small regions. Such subdivision of space is known as mesh, grid or cell division. The cell division is illustrated in the table 3.1 from the previous section. In addition, the number of threads per block of the CUDA code implementation are based on the FDTD cell division, the division are illustrated in table 3.3 and 3.4, which are based on the

equation 2.3 from chapter 2. To solve the Zhang-Li model 2.2 we need to determinate and evaluate the first and second derivate. The proposed solution is based on the seconds nearest neighbors. The basic idea is showed on the figure . The equation 2.3 is evaluated for the x, y and z coordinates.

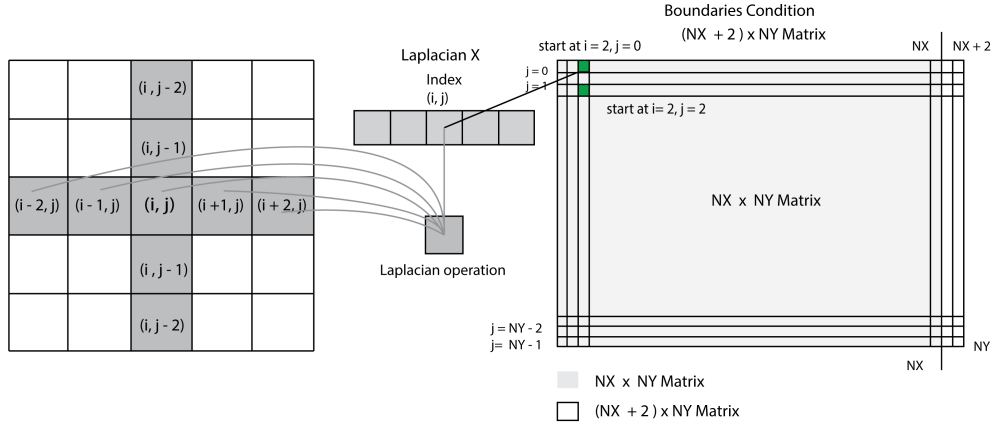


FIGURE 3.4: Laplacian XY block calculation and boundaries condition

As the figure 3.4 demonstrates the calculation of the nearest neighbors expansion by evaluation a neighborhood of  $[-2, 2]$  values in the x direction. In addition, the index begins at  $i = 2$  and finishes at  $NX + 2$ . The same occurs for the laplacian in the Y direction, however it begins at  $j = 2$  and finish at  $NY - 2$ . The implementation 3.5 uses the equation from chapter 3 2.3 as previous mention. The calculation 3.5 is done for each three x, y and z coordinates.

---

```

int i = blockIdx.x * blockDim.x + threadIdx.x + 2;
int j = blockIdx.y * blockDim.y + threadIdx.y;
// map the two 2D indices to a single linear, 1D index
int idx = j * grid_width + i;

lapy[idx] = -deltam[idx + 2] / 12.0 + 4.0 * deltam[idx + 1] / 3.0
            - 5.0 * deltam[idx] / 2.0
            - deltam[idx - 2] / 12.0 + 4.0 * deltam[idx - 1] / 3.0;

```

---

LISTING 3.5: Laplacian X using global memory

However, the calculation of the nearest neighbors only works for values of points inside a grid of  $[-2, 2]$  for x, y, and z coordinates. In addition, we need to calculate the boundaries values for those points that are in the edge of the grid, such as the beginning points and the end points. In other words close to the magnetization boundaries. To solve the boundaries issue we use two square matrices from chapter 2. The equation 2.7 for boundaries at  $j = 0$  and  $j = NY - 1$  for all values in the  $i$  cell, and the equation 2.6 for the condition  $j = 1$  and  $j = NY - 2$  for all  $i$  values. The code 3.6 demonstrate how the implementation was done, to achieve the correct values, first the laplacian in the y direction is calculated, then the boundary condition in the x direction.

---

```
--global__ void glaplaciany(...){} //Compute laplacian in Y direction

--global__ void glaplacianBoundaries(...){
    if (i > 1 && i < NX + 2 && j == 0){
        // Update Laplacian Boundaries Equation 3.10
    }
    else if (i > 1 && i < NX + 2 && j == 1){
        // Update Laplacian Boundaries Equation 3.9
    }
    else if (i > 1 && i < NX + 2 && j == NY - 2){
        // Update Laplacian Boundaries Equation 3.9
    }
    else if (i > 1 && i < NX + 2 && j == NY - 1){
        // Update Laplacian Boundaries Equation 3.10
    }
}
--global__ void glaplacianx(...){} //Compute laplacian in X direction
```

---

LISTING 3.6: Evaluation of Laplacian X, Y with boundary condition

The three CUDA kernels *glaplaciany*, *glaplacianx* and *glaplaciany* are evaluated for each x, y and z coordinate. In addition, the three coordinate sum up to 172,800 cell points to be calculated.

### 3.1.3.2 Zhang and Li Model

The Zhang-Li Model 2.2 is solved using code 3.8. Furthermore, the Zhang-Li equation is used as function *f* for the RK4 integration process 2.8. The first term of the equation *sfrrelax* is calculated in the relaxation process at the end of the RK4 integrator ???. Then the term *sdex* is computed in the Cross Product process, which is done before the RK4 calculation. The matrix *sm* is only calculated once at the initial calculations process, kernel *gsource* in the code 3.3. Finally, the *lapl* matrix is evaluated in the Laplacian process. Moreover, computing the Laplacian for x, y coordinate of the CUDA memory grid. The same process evaluates the Laplacian boundary condition, using the FDTD method.

---

```
sfrrelax[idx] = -deltam[idx] / tau_sf;
sdex[idx] = -(deltam[idx] * m[index] - deltam[idx] * m[idx]) / tau_sd;

//Evaluate Zhang - Li Method
solveZhangLi[idx] = sfrrelax[idx] + sdex[idx] + lapl[idx] - sm[idx];
```

---

LISTING 3.7: Runge and Kutta 4th Terms

Once completed the evaluation of the Zhang-Li Model (listing 3.7), The matrix *solveZhangLi* is assigned to each one of the RK4 terms evaluation.

### 3.1.3.3 Runge and Kutta

Intuitively the equation 2.8 is implemented by using four CUDA kernels, each kernel calculates the step of the integration. The first part of 3.8 computes the Runge and Kutta's 1st, 2nd, and 3rd term 2.9. The final fourth term, is the sum of the previous 3 terms, the last two lines of code in 3.8 show the calculation.

---

```

rk1[idx] = dt * deltam[idx]; // Terms k1, k2, k3
deltam[idx] = temp[idx] + 0.5 * rk1[idx];

rk4[idx] = dt * deltam[idx]; //final k4
deltam[idx] = temp[idx] + (rk1[idx] + 2.0 * (rk2[idx] + rk3[idx])
                           + rk4[idx]) / 6.0;

```

---

LISTING 3.8: Runge and Kutta 4th Terms

On each RK4 step the Zhang-Li model is evaluated, Moreover, numerically solving the model with the FDTD method including the magnetization boundaries condition.

The integration is group up in two *for* cycles (listing3.9). The inner *for* cycle evaluates the RK4 for the x, y, z coordinate. The outer for cycle evaluates four times the Runge and Kutta integration.

---

```

for(int term = 0; term < 4; term++)
    for(int coord = 0; coord < 3; coord++)
        gsd_exchange<<<blocks, threads>>>(term, coord);
        glaplacianx<<<blocks, threads>>>(term, coord);
        glaplacianyboundaries<<<blocks, threads>>>(term, coord);
        glaplaciany<<<blocks, threads>>>(term, coord);
        gsolution<<<blocks, threads >>>(term, coord);
        gterm_RK4<<<blocks, threads >>>(term, coord);
}

```

---

LISTING 3.9: Summarize of Runge and Kutta 4th Integration

Consequently the simulation is set to 50,000 iterations of the previous numerical methods ( simulation flow 3.1). However, is possible for the simulation diverge, and yield to inconsistent results.

### 3.1.4 Calculate effective beta

The RK4 algorithm 1 will finish until the beta evaluation reaches the value of  $1.0e^{-9}$ . The final step of the simulation determinate the effective beta, which tells use the energy configuration of the system. But more importantly the spin diffusion. Furthermore, the DW velocity the diffusion non-adiabatic term  $\beta$ .

The kernels 3.10 are launched only when the RK4 integration is done evaluating. The effective beta kernels computes a single value, the effective beta.

---

```
gm_x_sm << <blocks, threads >> >(...); //Calculate
gu_eff << <blocks, threads >> >(...); //Calculate
gu_eff_beta_eff << <blocks, threads >> >(...); //Calculate
gbeta_eff << <blocks, threads >> >(..); //Calculate
gbeta_diff << <blocks, threads >> >(...); //Calculate
```

---

LISTING 3.10: Calculate effective beta

We do not know for how long we need to integrate the system. However, it will stop until the local energy reaches the minimum configuration. Hence, the effective beta diverges to  $1^{-9}$ . The simulation will stop when the effective beta reaches the minimum. Then the magnetization data is written. Depending on the application configuration is possible to write either the magnetization results for the VW or for the ATW. The magnetization data is written into two separated data files, which contains the effective data .eff and the spin accumulation data .spin.

## 3.2 Validation

Because CUDA framework is highly parallel system is fairly easy to obtain erroneous data from the calculations, even setting up the threads per block incorrectly is possible to get data set that is wrong, or results that don't diverge. When making changes to the code, its is necessary to validate the new code.

The validation is done by comparing the output of the simulation with a valid data set, the output of the validation application tells us the error factor of the current data with the valid set. So for each data set there is a threshold value, that can tell if the that is close enough to the results. A example of the validation performed.

According to our results, new code shouldn't produce errors in the spin.dat data greater than  $7.0^{-17}$ , in other words valid code don't lead to differences greater than the precision expected from computations with double precision  $1.0^{-16}$  in the case of eff data the errors are in the order of  $1.0^{e-11}$  and no greater than  $6^{-11}$ . For the diffuse beta variation the precision expected to be within the double precision range of  $1^{-16}$ .

The initial implementation results were done using the GeForce GT 650M, with 384 CUDA core at 745 MHz and 2GB GDDR5 of memory. The final simulation with a correct validation data outputs the following results 3.5. The 1.00x speedup is used for comparing optimization results in the final chapter 5.

| Data set            | Simulation time | Speedup | Diffuse beta          |
|---------------------|-----------------|---------|-----------------------|
| upVW magnetization  | 377590.3ms      | 1.00x   | 4.848728452719814e-02 |
| ATWpm magnetization | 377409.2ms      | 1.00x   | 4.054674178687585e-02 |

TABLE 3.5: Calculation results

To conclude, the simulating at its core uses the RK4 for integration which uses as integration function the Zhang-li model equation 2.2. In addition, to solve such differential equations of the Zhang-Li model the FDTD method is evaluated. For each iteration the RK4 2.8 evaluates fourth times the Zhang-Li equation. Moreover, each term evaluates numerically the laplacian 2.3 and boundaries conditions 2.7 2.6. We showed the procedure of numerically solving the equations from Chapter 3.

## Chapter 4

# Heterogeneous Performance Analysis and Practices

Working with GPUs new challenges emerges, how can we make the best usage of the GPU hardware. In the conventional CPU model, we have what is called linear or flat memory model. In addition this appears to the programmer as a single contiguous address space. Furthermore, the CPU can directly address all the available memory, in other words there is almost no efficiency penalty in creating global data, local data, or even access data that is located on a opposite memory location, all of this can be access as a contiguous block [6]. Meanwhile, on the GPU there are exceptions, their exists different memory hierarchies which dramatically change the performance output. By allocation the optimal memory types, speedup and increase throughput can be accomplished. To ensure optimization, some analysis should be done, such as comparing latency, memory hierarchies and data bandwidth between CUDA kernels. Debugging of parallel code can be accomplish using the NVIDIA's Visual Profiler. The current chapter demonstrated techniques, practices and methods to debug and analyzed parallel process on NVIDIA's GPUs.

### 4.1 Practices

There are three rules for developing high performance GPGPU (General-purpose on the GPU) program, which are based on NVIDIA's GPU standards [8].

1. Get the data on the GPU device and keep it there
2. Process all the data en the GPU, give it enough work to do.

3. Focus on data reuse within the GPU context, to avoid memory bandwidth limitations

As we know the GPUs are plugged into the PCI Express bus of the host computer, in other words the CPU. The PCIe bus has extremely slow bandwidth compared with the GPU. This is why it is important to store the data on the GPU and keep it busy. In addition minimize the data transfer from the host and back to the device. We can see this in the table 4.1. CUDA enables the GPU to carry out petaFLOP performance in a single device [6]. In addition they are fast enough to compute a large amount of data. To accomplish such high performance, each CUDA Kernel needs to use all the available resources of the GPU. Furthermore, avoid wasting compute cycles. Finally if a single Kernel doesn't use all of the available bandwidth, multiple kernels can be launched at the same time on a single GPU, which are streams [8].

|                             | Bandwidth (GB/s) | Speedup over PCIe Bus |
|-----------------------------|------------------|-----------------------|
| PCIe x16 v2.0 bus (one-way) | 8                | 1                     |
| GPU global memory           | 160 to 200       | 20x to 28x            |

FIGURE 4.1: PCIe bus and GPU bandwidth comparison [6]

The practices should be taken in consideration to identify the portions of code where it would be beneficial for improving GPU acceleration [21].

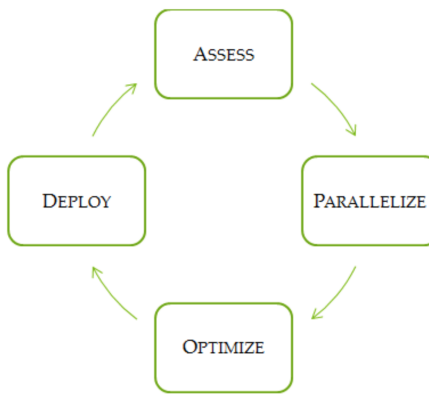


FIGURE 4.2: GPU application practices [21].

### Asses

The first step is to locate the part of the code where the majority of the execution time occurs. The programmer can evaluate memory bottlenecks for GPU parallelization.

### Parallelize

Increase parallelization from the original code, could be either adding GPU-optimized

libraries such as cuBLAS, cuFFT, or including more amount of parallelism exposure though the use of CUDA code.

#### Optimize

The developer can optimize the implementation performance through a number of considerations, overlapping kernel executing, kernel profiling, memory handling and fine-tuning floating-point operations.

#### Deploy

Compare the outcome with the original expectation. Determinate the potential speedup by accelerating a given section. First a partial parallelization should be implementation before carrying out a complete change.

## 4.2 Performance Metrics

There are many possible approaches to profiling the code, but in all cases the objective is the same: identify the kernel or kernels in which the application is spending most of its execution time and increase the throughput by a giving kernel. Throughput is how many operations completed per cycle.

### 4.2.1 Timing

Timing a launched kernel can be done on either the GPU or the CPU. Is important to remember that the CPU and GPU are not synchronized. So its necessary to synchronize the CPU thread with the GPU kernels launches. CUDA provides the required functions to synchronize the CPU with the GPU calling immediately before starting the timer [21]. CUDA is able to handle timers within the GPU, which records times in a floating-point value in milliseconds. This is done with *cudaEventRecord()*, just by including *start* and *stop* in the function inputs. Note that the timing are measured on the GPU clock, so the timing is independent from the OS [6]. The timing performed on the application is showed in Chapter 5.

### 4.2.2 Bandwidth

The bandwidth refers to the rate at which data can be transferred between host and device and vice-versa. The bandwidth is one of the most important factors for testing performance o the GPUs. Choosing the right type of memory could dramatically increase performance and bandwidth. There are two main bandwidth types to indicate

performance, theoretical bandwidth and effective bandwidth. The theoretical bandwidth is base on the hardware specifications that is available by NVIDIA. This is calculated using the following formula:

$$\text{theoretical bandwidth} = (\text{clockrate} * (\text{bit-wide memory interface}/8) * 2)/10^9$$

For example the NVIDIA GeForce GTX 280 uses DDR RAM with a memory clock rate of 1,105 MhZ and a 512-bit-wide memory interface

$$(1107 * 10^6 * (512/8.0) * 2)/10^9 = 141.6 \text{Gb/sec}$$

The GTX 280 has a theoretical bandwidth of  $141.6 \text{Gb/sec}$ . The effective bandwidth is calculated by timing specific program activities and by knowing how data is accessed by the application [21].

$$\text{effective bandwidth} = ((\text{Br} - \text{Bw})/10^9)/\text{time}$$

Where Br is the number of bytes read per kernel, Bw is the number of bytes written per kernel and t is the elapsed time given in seconds [28].

In practice the difference between theoretical bandwidth and effective bandwidth indicated how much bandwidth is wasted on accessing memory and calculations. If the effective bandwidth is low compared to the theoretical bandwidth is one indication that there is not enough work being done in the GPUs. In addition, there are several solutions; analyze the code to make more parallelize instructions, execute more computational instructions on the GPUs, finally analyze the number of threads per block that are executing on execute kernels.

The next chapter we analyze the bandwidth and timing for each NVIDIA GPU card used to optimize the application. However, the bandwidth information is only available for analysis when transferring data from the CPU to the GPU or vice-verse.

### 4.3 Memory Handling with CUDA

In this section four types of memory handling are going to be explained, global memory (device memory), shared memory, texture memory and constant memory. The figure 4.3

illustrates physically the position of the different memory types inside the device chip.

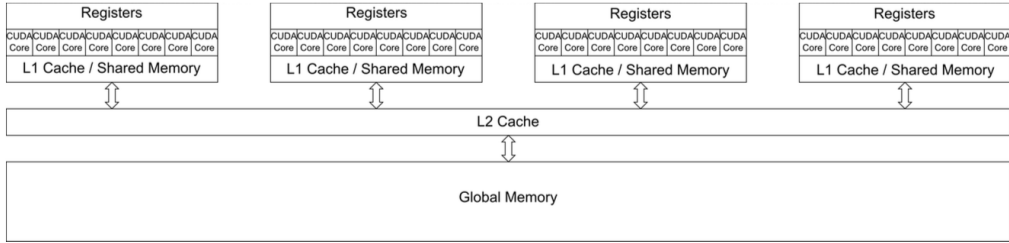


FIGURE 4.3: The schematic cache hierarchy of a CUDA GPU with 4 Streaming Multiprocessors and 8 CUDA Cores each [6].

Global memory is very large in comparison to the shared memory, which is on the L1 cache. However, the global memory is far away from the registers and from the CUDA core locations. Moreover, the memory access is very slow in comparison to the shared memory [6].

The table 4.4 illustrates the five different memory types that are available in CUDA. But more interesting the bandwidth penalty and the latency in computer cycles for each one of them. Moreover, different memory types can be used in different applications to maximize performance, hence memory usage. The Shared Memory is very limited so it cannot be handled across all situations. Furthermore, implementing a wrong memory type on the device there are possibilities for latency penalties and bandwidth drop, instead of having a performance gain.

| Storage Type | Registers | Shared Memory  | Texture Memory | Constant Memory | Global Memory |
|--------------|-----------|----------------|----------------|-----------------|---------------|
| Bandwidth    | ~8 TB/s   | ~1.5 TB/s      | ~200 MB/s      | ~200 MB/s       | ~200 MB/s     |
| Latency      | 1 cycle   | 1 to 32 cycles | ~400 to 600    | ~400 to 600     | ~400 to 600   |

FIGURE 4.4: Different memory type and penalties usage [6]

### 4.3.1 Global Memory

Understanding how efficiently use global memory is essential part of CUDA memory management. Focusing on data reuse within the SM and caches avoids memory bandwidth limitations. Global memory on the GPU is designed to quickly stream memory blocks of data into the SM [8].

- Get the data on to the Device, keep it there.
- Give the GPU enough workload, this using all the resources available from the GPU.

- Focus on data reuse within the GPGPU to avoid memory bandwidth limitations.

In other words the global memory resides on the device, and it should be anything from 1 byte to 8GB, depends on the GPU RAM available. Furthermore, the memory is visible to all the threads of the grid. Every thread at a given location is possible to read and to write global memory, The memory is always allocated with the keyword *cadaMalloc*. In addition, the global memory is only used by passing it to the kernel call the keyword *\_global* . Global memory is widely used for the current implementation [8].

### 4.3.2 Shared Memory

CUDA C compiler treats variables differently than a typical c variable, it creates a copy of the variable for each block that is launched on the GPU, now every thread in that block can access the memory, this is why is called shared memory. This memory reside physically on the GPU, because the memory is very close the cache, the latency is typical very low [29]. One thing comes to mind, if the threads can communicate with others threads, so there should be way to synchronize all the threads. A simple case should be if thread A writes a value into the shared memory, and Thread B wants to access we need to synchronize, when thread A finish writing then Thread B can access it. This is typical case when shared memory with synchronize thread is needed [6].

Shared memory is magnitudes faster to access than global memory, essentially is like a local cache for each threads of a block. While the shared memory is limited to 48K a block, the global memory is the amount of DRAM on the device. The duration of the shared memory on the device is the lifetime of the thread block. Using *\_shared* *\_in-front* of the data type will innovate shared memory.

Shared memory is widely used for applications were the kernels access a great amount of global memory. In addition, using shared memory eliminates the use of clock cycles per kernel which increases performance on a single kernel call. For the current application we used extensively shared memory, eliminating the use of global memory. More information about the process in Chapter 5.

### 4.3.3 Constant Memory

Is an excellent way to store and broadcast read-only data to all the threads on the GPU. One thing to keep in mind is that the constant memory is limited to 64KB [8]. A simple analogue is the *#define* or *const* attribute in the C++ programming language, the variable performs like a variable that cannot be modified. On CUDA this is exactly

the same, the value can only be read and not written. Furthermore, the value will not change over the course of a kernel execution and only the host can write the constant memory [29]. Please read Chapter 5 for speedup improvements by increasing the use of constant memory.

#### 4.3.4 Texture Memory

Like constant memory, texture memory is another variety of read-only memory that can improve performance and reduce memory traffic when reads have certain access patterns. Traditionally texture memory is used for computer graphics applications, but it can also be used for HPC. The main idea of this read-only memory is that threads are likely to read from address "near" the address they nearby threads [29].

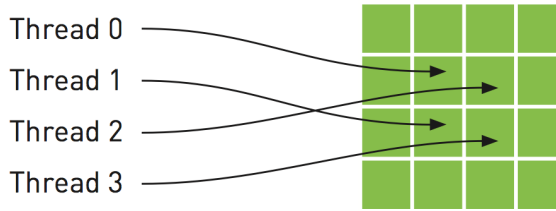


FIGURE 4.5: Mapping of threads into a two dimensional array of texture memory [15]

The texture Memory in a form works like the GPU graphics Texture, when you want to use the texture bind with some sort of data is necessary and when you finish using it unbind the texture from the data. The usage can be summarized in the following table:

- Allocate global memory in the Host.
- Create Texture reference and bind it to memory object.
- On the device obtain the reference from the texture.
- Use Texture memory operations on the device
- When the work is done on the Texture, unbind the texture reference on the host.

The texture memory is not used on the current implementation, for obvious reasons, it is a read only memory. For the current application we need to constantly read and write blocks of memory.

### 4.3.5 Thread Synchronization

This refers to synchronizing threads operations. For efficiency, a pipeline can be created by queuing a number of kernels to keep the GPGPU busy for as long as possible. Further, some form of synchronization is required so that the host can determine when the kernel or pipeline has completed [8]. Commonly used synchronization mechanisms are:

- Explicitly calling `cudaThreadSynchronize()`, which acts as a barrier causing the host to stop and wait for all queued kernels to complete.
- Performing a blocking data transfer with `cudaMemcpy()` as `cudaThreadSynchronize()` is called inside `cudaMemcpy()`.

The basic unit of work on the GPU is a thread. It is important to understand from a software point of view that each thread is separate from every other thread. Every thread acts as if it has its own processor with separate registers and identity. Will wait for all threads to finish there job [8].

Threads synchronization can also be accomplish inside of the kernels calls. The idea is the same, the kernel will wait until all the threads have completed there task. When more threads are synchronize they schedule more work, hence, better performance and more workload. Threads synchronization is general used when loading data into shared memory. The implementation of such process is in Chapter 5, section optimizations.

## 4.4 Concurrent Kernels

Kernels are executed in a sequential form with parallel instructions. In addition, with CUDA's streams is possible to launch several kernels in parallel, in other words, overlap kernel in the same launch sequence. As the figure 5.3 illustrates.

A stream in CUDA is a sequence of operations that execute on the device in the order in which they are issued by the host code. Every kernel is launch on the default stream zero. Hence, to overlap kernel execution, non-default streams should be used for every kernel launch. To accomplish concurrent kernels, streams should be pinned to a non-default stream (non zero)[15].

Using two or more CUDA streams, we can allow the GPU to simultaneously execute a kernel while performing a copy between the host and the GPU. We need to careful about two things. First, the host memory involved needs to be allocated, since we will queue our memory copies, we need to synchronize those copies. Second. we need to be

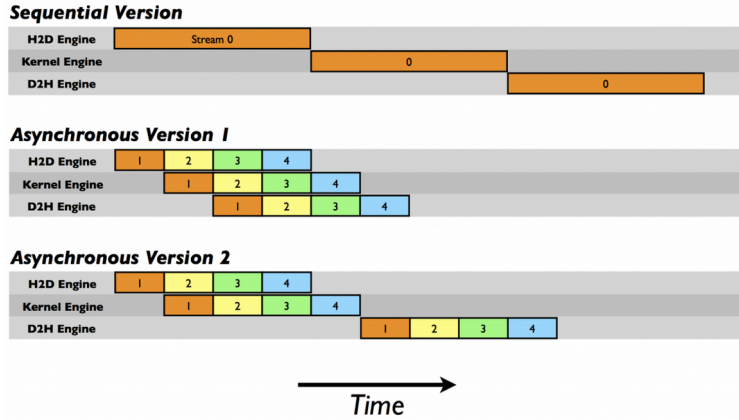


FIGURE 4.6: Overlapping kernel execution using CUDA streams

aware that the order in which we add operations to our streams will affect our capacity to achieve overlapping of copies and kernel execution. The general guideline involves a breadth-first, or round robin, to assign work and queue work to the kernels [29].

Concurrent kernels is technique which is implemented in this application. In addition, the order of kernel execution effected the operations of the streams. Moreover, Chapter 5 illustrates the path taken to accomplish such task.

## 4.5 Kernel Analysis

Kernels are the essential part of CUDA programming, threads are launched automatically throughout each thread per blocks of the device. Furthermore, millions of threads execute the same code in parallel. However, the parallel code can be bound by three factors memory, compute and latency [6].

### Memory Bandwidth Bound

Refers to code/application is limited by memory access. Most GPUs card have 1GB- 6GB of memory, which is used to process the data on the GPU. Different solutions are: reuse data, use different GPU memory types, implement a multi-GPU approach to increase the memory.

### Compute Bound

Refers to the computation time execution, in other words calculations done in the device, under the assumption that there is enough memory for the calculations. This is the number of operations per cycle on the kernel. Theoretical bandwidth vs effective Bandwidth can measure performance for a compute-bound Kernel. Therefore, it is possible to increase the FLOPS per device.

### Latency Bound

Is one whose predominate stall reason is due to memory fetches. This is actually the saturating the global memory, or any type, but still have to wait to get the data into the kernel. Physically, is data being sent from one part of the device to the other. Also depends the time required to perform an operation, and are counted in cycles of operations. A way to reduce the latency is to increase the number of parallel instructions (more calls per thread), in other words more work per thread and fewer threads. However, this is not always possible.

Depending on the problem, the application can be bound by the previous three factors. The next chapter we are going to explain how and why the current implementation is bounded by memory, compute and latency.

## 4.6 Hardware constraints

Depending on the hardware capabilities limits how many threads per block a kernel launch can have. If exceed this values, the kernel will run incorrectly. The threads per block depends of the GPU hardware capabilities. The compute capabilities of a device is represented by a version number, also sometimes called its "SM version". This version number identifies the features supported by the GPU hardware and is used by applications at runtime to determine which hardware features and/or instructions are available on the present GPU [22]. In a roughly summarized as:

- Each block cannot have more than 512/1024 threads in total. (Capability 1.x or 2.x-3.x)
- The Maximum dimensions of each block are limited to [512,512, 64]/[1024, 1024, 64](compute 1,1.2)
- Each block cannot consume more than 8k, 16k, 32K registers total
- Each block cannot consume more than 16kb/48kb of shared memory

Another inefficiency that can cause low performance in the CUDA application, is the number transfers memory calls between the CPU and the GPU. The GPU communicates with the CPU via a *PCIe* bus as mentioned before. In addition, all of the massive FLOPS per second that can be achieve in the CPU cannot be sent back to the CPU. Because of the physical connection between the GPU and CPU. The GPU should be filled up with enough workload at the beginning of the application and only at the end return the

memory back to the CPU. However, this is not always possible, a technique to increase more throughput from this operations is to pin the memory in the host. But also send as much data as possible in a single kernel call by using the maximum the GPU hardware capabilities [21]. For the current implementation, CPU and GPU is relatively low, only a few times communication is done by the device and host.

#### 4.6.1 Thread Division

There are hardware limitations in how much threads per block a kernel can handle. Launching a kernel with the hardware constraints of the device will only ensure us that the kernel will actually be executed in the device. Nonetheless, not 100% optimal and the results can be incorrect. Furthermore, it is necessary to launch kernels with the amount of threads per block base on the hardware settings. The block size will determine how faster the code will run. However, not the biggest block will run faster, depends on the problem and the data set. By Benchmarking the application, is possible to find the optimal configuration that best fits the problem. One thing to keep in mind, thread blocks should be a multiple number of SMs, with this idea is possible to obtain optimal thread block configuration. See Chapter 5 for the optimal thread configuration for the application. The optimal number of threads per block did not occur on the maximal available threads per block of the devices.

### 4.7 Visual Profiler

Is a hard task to keep track of each individual thread. This becomes difficult for debugging highly parallel applications. The NVIDIA's Visual Profiler is a profiling tool that can be used to measure performance and find potential opportunities for optimization in order to archive maximum performance on the GPUs. The Profiler provides metrics in the form of plots and graphs, which describes opportunities to fully utilize the compute and data movements capabilities of the GPU, as well of each kernel launch in the application. See Figure 4.7.

NVIDIA's profiling tools comes in various flavors; a standalone profiler through the visual profiler compiler nvvp, integrated in a GUI NSight Eclipse Edition as NSight command (Visual Profiler), and as a command-line profiler though nvprof command. Each one has its disadvantages and advantages. The command-line profiler is useful for remotely access, where a GUI is not available, while the NSight can show graphs, plots and timeline of the application. The Profiler support CUDA applications as well as openCL applications. However, there are exceptions.

|  | Transactions | Bandwidth   | Utilization   |
|--|--------------|-------------|---|
| <b>L1/Shared Memory</b>                    |              |             |   |
| Shared Loads                               | 0            | 0 B/s       |   |
| Shared Stores                              | 0            | 0 B/s       |   |
| Shared Total                               | 0            | 0 B/s       |  Idle Low Medium High Max |
| <b>Texture Cache</b>                       |              |             |   |
| Reads                                      | 0            | 0 B/s       |  Idle Low Medium High Max |
| <b>L2 Cache</b>                            |              |             |   |
| Reads                                      | 97364        | 24.654 GB/s |   |
| Writes                                     | 97201        | 24.613 GB/s |   |
| Total                                      | 194565       | 49.267 GB/s |  Idle Low Medium High Max |
| <b>Device Memory</b>                       |              |             |   |
| Reads                                      | 87840        | 22.243 GB/s |   |
| Writes                                     | 90092        | 22.813 GB/s |   |
| Total                                      | 177932       | 45.056 GB/s |  Idle Low Medium High Max |
| <b>System Memory</b>                       |              |             |   |
| [ PCIe configuration: Gen3 x16, 8 Gbit/s ] |              |             |   |
| Reads                                      | 0            | 0 B/s       |   |
| Writes                                     | 5            | 1.266 MB/s  |   |
| Total                                      | 5            | 1.266 MB/s  |  Idle Low Medium High Max |

FIGURE 4.7: Profiler provides optimization metrics necessary to improve the application.

The Visual Profiler, by default, will execute the entire application, nonetheless typically only some parts of application only need performance optimization. This enables to determine kernels, code where critical performances is needed. The common situations where profiling a region of the application is helpful [22].

- Analyze data initialization and movement in the CPU and GPU, as well as evaluating CUDA calls.
- The application operates in phases, where a algorithm operates throughout each region. The application can be optimized independently from other phases of the code.
- The application contains algorithms that operate though a large number of iterations. In this case is possible to collect data from a portion of the iterations.

The Visual Profiler provides a step-by-step optimization guidance, where is possible to evaluate the GPU usage, examine individual kernels and analyze timeline of the application which the profiler shows memory movements and usage, CUDA calls, number of threads and performance. The figure 4.8 shows, each Kernel has its own percentage of execution time of the overall application [21].

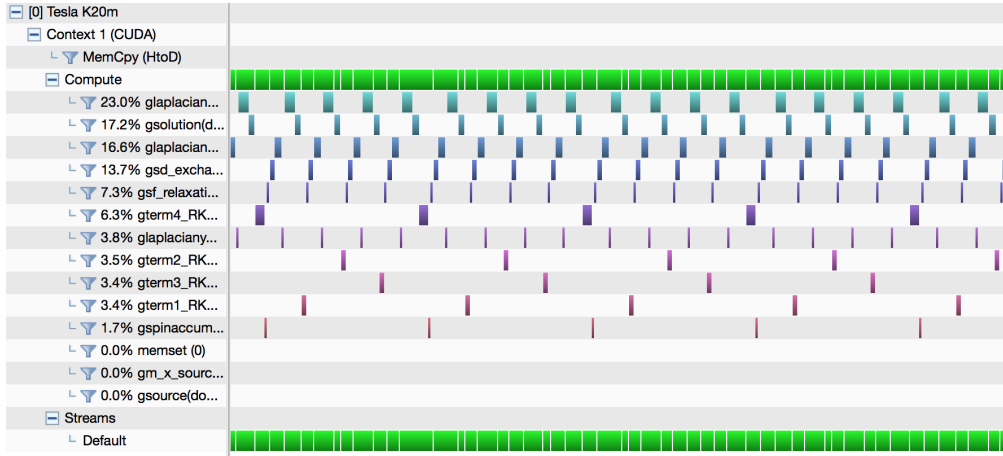


FIGURE 4.8: Visual Profiler kernel execution, and timeline execution

### 4.7.1 Profiler Kernel Report

The profiler will execute several times the application for it to collect data from each kernels. This enables to precisely optimize phases of the application[29]. The profiling tools can verify how long the application spends executing each kernel as well the number of used blocks and threads. Through this is possible to obtain various memory throughput measures, like global load throughput and global store throughput, indicate the global memory throughput requested by the kernel and therefore corresponding to the effective bandwidth mentioned in the last section.

As we know the profiler executes the application several time to collect data about each kernel. The information obtained by each kernel can be sum-up in-to a report that can be exported in a pdf file, which has the following information.

#### 1. Compute, Bandwidth, or Latency Bound

The performance determines if the kernel is bounded by computation, memory bandwidth, or instructions/memory latency. It shows how is limiting the performance respectively.

#### 2. Instructions and Memory Latency

Instruction and memory latency limit the performance of a kernel when the GPU does not have enough work to keep busy. The performance of latency-limited kernels can often be improved by increasing occupancy. Occupancy is a measure of how many warps the kernel has active on the GPU, relative to the maximum number of warps supported by the GPU.

#### 3. Compute Resources

GPU compute resources limit the performance of a kernel when those resources are

insufficient or poorly utilized. Compute resources are used most efficiently when instructions do not overuse a function unit.

#### 4. Floating-Point Operation Counts

floating-point operations executed by the kernel, can be either single precision or double precision.

#### 5. Memory Bandwidth

Memory bandwidth limits the performance of a kernel when one or more memories in the GPU cannot provide data at the rate requested by the kernel.

The profiling report was used in the current implementation to optimize the CUDA code. More about the results read Chapter [5](#).

#### 4.7.2 Collect Data On Remote System

As mention before, is possible to collect data from a remote system where a GUI is not available, using the command-line nvprof. Remote profiling is the process of collecting profile data from a remote system that is different than the host system at which that profile data will be viewed and analyzed. Once the data is collected is possible to access the data using the Visual profiler, which enables a GUI and more compressive information about the application. There are two ways to perform remote profiling. To use nvvp remote profiling you must install the same version of the CUDA Toolkit on both the host and remote systems. It is not necessary for the host system to have an NVIDIA GPU [\[22\]](#). For the current application, remote profiler was used. However, the server did not have an external monitor or virtual. Therefore we could not obtain all the profiling analysis. Moreover we use a local laptop for profiling.

Finally, this chapter gives a overview of practices and performance studies for GPGPU. In addition, a better understanding of the hardware and memory management on the GPU. As well as hardware limitation, which determinate the best usage of the GPUs. NVIDIA's profiling tools is a useful to analyze different stages of our application. Moreover, to determined which parts of the CUDA code is better to optimize from others, this is to gain a better performance in a small time frame.

## Chapter 5

# Optimization Results

This chapter are the results of the CUDA code implementation launched on a single GPU device. The tests were performed on various GPUs architectures. The application is analyzed on various stages using NVIDIA’s Visual Profiler. In addition, the CUDA kernels were evaluated in performance, execution time, occupancy and concurrent kernels. Furthermore, the results, are analyzed and optimized using the schemes from Chapter 4. The code is executed remotely on the supercomputer “Piritakua” at the Department of Multidisciplinary Studies Yuriria, University of Guanajuato. The last section is the overview of all the optimizations results performed on the simulation.

### 5.1 Supercomputer “Piritakua”

The experiments are carried out using the supercomputer Piritakua. The massive GPU cluster was design and built by Dr. Claudio from the University of Guanajuato at Yuriria’s Multidisciplinary Studies. The GPU cluster is located at a small town of Mexico, Yuriria. The supercomputer at the front-end has a eight core Intel Xeon at 2.4 Ghz, at the back-end several GPU are connected. All of GPUs CUDA version 5.0 was installed. Furthermore, the GPUs node are; one NVIDIA Tesla K20, two Tesla M2070 and a GeForce GTX 580

The cluster has a GNU LINUX distribution installed, the CentOS 64 bits version 6.4. CentOS stands for Community Enterprise Operating System which is free operating system and one of the most popular GNU Linux distribution for web servers and as well is supported by RHEL (Red Hat Enterprise Linux) [3]. The specifications of the front-end cluster are 5.1.

| Processor   | Number | Cores | RAM    |
|---|--------|-------|--------|
| Server Dell Intel Xeon E5620 2.4 GHz                        | 1      | 8     | 12 GB  |
| Server HP Proliant SL 350s Gen3 Intel Xeon X5650 2.67 GHz   | 2      | 24    | 32 GB  |
| Server HP Proliant SL 250s Gen8 Intel Xeon E5-2670 2.60 GHz | 3      | 48    | 104 GB |
| CPU Xeon Phi 5110p  | 1      | 8     | 8 GB   |
| CPU Xeon Phi 7120p  | 1      | 8     | 16 GB  |

TABLE 5.1: CPU specifications

The CUDA Code was launched on only two CPUs, a laptop with a eight core intel i7-3630QM and a high-end CPU Xeon Phi 7120p from the cluster. In addition the Xeon Phi was used for all the experiments for the Cluster's GPUs. The Xeon Phi 720p is capable of achieving f 1.2 teraflops of double precision floating point instructions with 352 GB/sec memory bandwidth at 300 W. The code was executed on laptop to show the performance comparison between a lightweight GPU and a server based GPU.

When accessing "Piritakua" remotely is possible to use all the GPUs nodes available on the cluster. The specifications of the GPU connected to the back-end are as follow, CC stands for compute capability.

| Model         | Core | RAM   | DP GF | SP GF | Bandwidth | GHz  | CC  | Power |
|---------------|------|-------|-------|-------|-----------|------|-----|-------|
| Tesla K20m    | 2496 | 5GB   | 1,170 | 3,520 | 208GB/s   | 0.73 | 3.5 | 225W  |
| Tesla M2070   | 448  | 6GB   | 515   | 1,030 | 150GB/s   | 1.15 | 2.0 | 225W  |
| Tesla C2050   | 448  | 2.5GB | 512   | 1,030 | 144GB/s   | 1.15 | 2.0 | 238W  |
| GeForce 580   | 512  | 1.5GB | 520   | 1,154 | 192.2GB/s | 1.5  | 2.0 | 244W  |
| GeForce 670mx | 960  | 3GB   | 520   | 1,154 | 67.2GB/s  | 0.6  | 3.0 | -     |

TABLE 5.2: GPU technical specifications

The code was launched on all Piritakua's GPUs and on an external GeForce GTX 670m, located on a laptop. The "m" stands for the mobil graphic cards. In addition the 670m card is design for less power usage, but with high graphics power, it even has more cores than some Tesla models, However, this types of cards has way more less Bandwidth than standard versions. The 670m card was used as comparison between laptop GPUs and high-end desktop/servers GPUs.

### 5.1.1 Architecture Differences

Architecture dependent technical differences of NVIDIA GPUs. During the CUDA development a lot of internal features have been improved, but most paradigms for the programmer stayed the same. For example a streaming processor can now handle 2048 threads at a time, but the maximum block size stayed at 1024. This results in a 100%

theoretical occupancy for block sizes of 1024 compared to 66% of Fermi. Another example is the use of Shared Memory. Maxwell has 64KB dedicated Shared Memory. The maximum amount of Shared Memory per Block is 48KB for all three architectures [10].

There are two GPU architectures where the implementation was launched, the Fermi and the Kepler. The Tesla K20m and the GeForce 670mx are based on the “Kepler” GPU architecture. The Tesla M2070, M2050 and the GeForce GTX 580 on the Fermi architecture. The Kepler architecture newer than the Fermi. More information about the architectures in the table 5.3. The Maxwell architecture wasn’t used for benchmarking test. However, it is showed for future reference and analysis.

| Name                                     | Fermi             |     | Kepler      |                   | Maxwell        |
|--|-------------------|-----|-------------|-------------------|----------------|
| Compute Capability                       | 2.0               | 2.1 | 3.0         | 3.5               | 5.0            |
| Single Precision Operation per Clock/SIM | 32                | 48  | 192         |                   | 128            |
| Double Precision Operation per Clock/SIM | 4/16 <sup>1</sup> | 4   | 8           | 8/64 <sup>2</sup> | 1 <sup>3</sup> |
| Max Number of Threads per SM / SM        | 16                |     | 32          |                   |                |
| Max Number of Registers per Thread/SIM   | 1536              |     | 2048        |                   |                |
| Max Number of Threads per Block          | 1024              |     |             |                   |                |
| Active Thread Blocks per SM / SM         | 8                 |     | 16          | 32                |                |
| Max Warps per Multiprocessor/ SM         | 48                |     | 64          |                   |                |
| Registers / SM                           | 32K               |     | 64K         |                   |                |
| Level 1 Cache                            | 16/48 KB          |     | 16/32/48 KB | 64 KB             |                |
| Shared Memory / SM                       | 16/48 KB          |     | 16/32/48 KB | 64 KB             |                |
| Warp Size                                | 32                |     |             |                   |                |

TABLE 5.3: GPU Architecture Specifications

## 5.2 Optimization

The CUDA code was launched on each one of ”Piritakua”’s GPUs. The supercomputer has different GPUs, as well as several different architectures. Furthermore, the initial results in time execution of the implementation are showed in figure 5.1. A GeForce GT 650M, with 384 CUDA core at 745 MHz and 2GB GDDR5 of memory is used as initial 1.00x speedup reference.

Using the NVIDIA’s Visual Profiler we obtain kernel metrics of the Tesla K20m. The output is organized by kernel performance throughout the simulation. For only the laplacian kernel evaluation; *glaplaciany*, *gLaplacianx* and *gLaplacianYBoundaries* uses up-to 44.37% of the overall simulation. The *gsolution* kernel, which solves Zhang-Li model 2.2 consumes up-to 14.04%. The RK4 integration only exhaust a minor part of the overall simulation. However, the *gSolution*, *gsdExchange* and laplacian calculation are part of the RK4 integration, which overall is about 99%.

The throughput was not review on the current application. Since only two stages of the simulation transfer of the CPU data occurs, on the initial stage where CPU data is sent to the GPU, and the final stage where is sent back to CPU.

The optimization focus is to give the GPUs as much work as possible, using at the fullest the GPU hardware capabilities. In addition, reducing the overall performance time of each kernel, eliminating the computational hover-head process on the highest consumed kernel 5.4.

| Time% | Time    | Calls | Avg     | Min    | Max     | Kernel                       |
|-------|---------|-------|---------|--------|---------|------------------------------|
| 23.50 | 3.6s    | 26521 | 137.5us | 96.0us | 597.1us | <i>gLaplaciany</i>           |
| 17.04 | 2.6s    | 26521 | 99.7us  | 57.0us | 561.1us | <i>gSolution</i>             |
| 16.75 | 2.6s    | 26522 | 98.0us  | 62.8us | 400.6us | <i>gLaplacianx</i>           |
| 13.37 | 2.0s    | 26522 | 78.2us  | 40.8us | 453.8us | <i>gsdExchange</i>           |
| 7.22  | 1.1s    | 26522 | 42.2us  | 23.4us | 326.0us | <i>gsfRelaxation</i>         |
| 6.22  | 965.2ms | 6630  | 145.6us | 79.2us | 722.6us | <i>gTerm4RK4</i>             |
| 4.12  | 640.3ms | 26522 | 24.1us  | 21.8us | 138.7us | <i>gLaplacianYBoundaries</i> |
| 3.41  | 529.2ms | 6630  | 79.8us  | 41.6us | 478.8us | <i>gTerm2RK4</i>             |
| 3.36  | 520.8ms | 6630  | 78.5us  | 41.5us | 372.2us | <i>gTerm3RK4</i>             |
| 3.35  | 519.5ms | 6631  | 78.3us  | 41.1us | 372.2us | <i>gTerm1RK4</i>             |

TABLE 5.4: Kernel time executing and on the Tesla K20

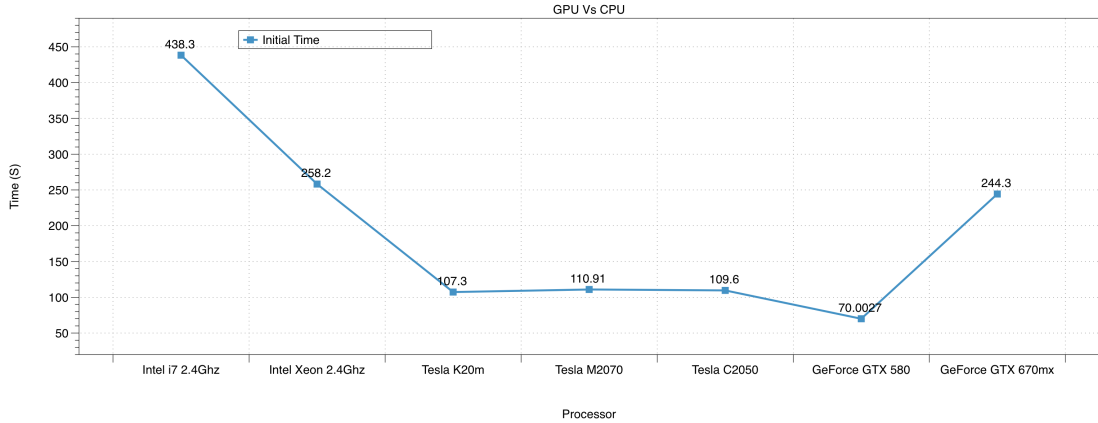


FIGURE 5.1: Initial implementation benchmarking on several different GPU nodes, speedup 1.0x

The figure 5.1 illustrate the GeForce GTX 580 is the card with the least amount of execution time, and the Tesla K20m the fastest amongst the Tesla Cards.

The following sections are the optimization techniques and methods applied to the application. In addition, comparing the performance between the initial implementation and the modified versions. The optimization is breakdown into five steps; Branching, Occupancy, Concurrent Kernels, Shared Memory and Structure of Arrays. Branching, refers how kernels and threads are executed in the application. Occupancy, number of

threads per devices being used. Concurrent Kernels, execution several kernels at once. Shared Memory, using as much shared memory as possible. Finally, Structure of Arrays, modification of the memory allocation in the device.

### 5.2.1 Branching

CUDA follows the Single Instruction Multiple Thread architecture. This means, threads execute the same code. Each thread can operate on its own data and has its own address counter. Moreover, threads are free to use a different path. Each thread launches the same operation at the same time. However, they have to wait for all the threads in the kernel to finish there task. In other words, some threads can finish their job before a groups of threads are still executing their task. When a thread within a warp branches differently the other threads get deactivated [10]. This can be described in the following code 5.1 and illustrated in the figure 5.2.

---

```
--global__ void kernel(int* out){
    idx = threadIdx.x;
    int result;
    if(idx == 0){
        result = foo();
    } else {
        result = bar();
    }
    out[idx] = result;
}
```

---

LISTING 5.1: Branching threads

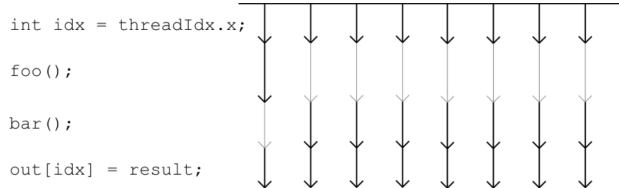


FIGURE 5.2: The execution flow of a branching code, with warp size 8. Black arrows are active threads, and the grey ones are disabled.

The branching problem occurred in the section where boundary condition for laplacian was being analyzed 5.2. Only a single kernel was used to check the boundary condition. In addition, a bottleneck occurred. The implementation gets the job done with only one kernel. However, a minor part of the threads are only working, which is a waste of computation resources and energy.

---

```
--global__ void glaplaciany(...); //Compute laplacian in Y direction
--global__ void glaplacianx(...); //Compute laplacian in X direction

--global__ void glaplaciannyboundaries(...){
```

---

```

if (i > 1 && i < NX + 2 && j == 0){
    // Update Laplacian Boundaries
}
else if (i > 1 && i < NX + 2 && j == 1){
    // Update Laplacian Boundaries
}
else if (i > 1 && i < NX + 2 && j == NY - 2){
    // Update Laplacian Boundaries
}
else if (i > 1 && i < NX + 2 && j == NY - 1){
    // Update Laplacian Boundaries
}
}
}

```

---

LISTING 5.2: Branching problem in the laplacian boundary condition evaluation

To solve the branching issue, we include more work on the laplacian boundary condition kernel. The new kernel evaluates the boundary condition in a single kernel. Therefore, eliminating branching threads, more importantly, reducing global memory calls (code 5.3).

---

```

__global__ void glaplacianyboundaries(...){
    if (i > 1 && i < NX + 2 && j == 0){
        // Update Laplacian Boundaries
    }
    else if (i > 1 && i < NX + 2 && j == 1){
        // Update Laplacian Boundaries
    }
    else if (i > 1 && i < NX + 2 && j == NY - 2){
        // Update Laplacian Boundaries
    }
    else if (i > 1 && i < NX + 2 && j == NY - 1){
        // Update Laplacian Boundaries
    }
    glaplaciany(...); //Compute laplacian in Y direction
    glaplacianx(...); //Compute laplacian in X direction
}

```

---

LISTING 5.3: More workload on a single kernel execution

The technique was applied to all parts of the code. Therefore, eliminated inactive threads. moreover, activating threads for computational process, the results of the modified version seek the Optimization Results section. The technique increased the occupancy percentage of active threads within the kernels.

### 5.2.2 Concurrent Kernels

Initially, each kernel was launched on the default steam zero. Therefore, every kernel was consequently launched in a serial way. The figure 5.3 illustrates such result using the

NVIDIA's Visual Profiler. Each kernel that is being launched cannot run simultaneously. Because, each kernel needs previous data to compute the next data. In other words, the kernels are not independent from each other. Therefore, we change the implementation to be able to launch parallel kernels.



FIGURE 5.3: Kernels running on the default Stream zero.

Kernels by default cannot run in parallel with others kernels. Furthermore, CUDA doesn't provide an automatic parallel kernel executing. In addition, the programmer needs to tell the CUDA compiler that some portion of the code or kernel should be run in parallel. However, the compiler cannot always execute concurrent kernels, depends on the hardware capabilities and as well the number of threads per block and the number of SM available. If the compiler finds available space to run another kernel simultaneously it will do so.

For example, the *gsolution* 5.4 kernel computes the Zhang and Li model for x, y, z coordinates, which extensively uses the global memory of the device. To achieve concurrent kernels, the streams should be able to access memory blocks that are pinned to specific a stream. Therefore, each memory block corresponding to x, y, z coordinate are mapped to 3 independent streams. Furthermore, all the matrices corresponding to the coordinate x are mapped to the stream 1, coordinate y to stream 2 and coordinate z to stream 3.

---

```
deltamX[index] = sfrelaxX[index] + sdexX[index] + laplX[index] - smX[index];
deltamY[index] = sfrelaxY[index] + sdexY[index] + laplY[index] - smY[index];
deltamZ[index] = sfrelaxZ[index] + sdexZ[index] + laplZ[index] - smZ[index];
```

---

LISTING 5.4: Evaluation of x, y, z coordinates of the Zhang and Li model in a single kernel.

The CUDA code 5.4 is divided into a single kernel 5.5. In addition this new generic kernel is launched parallel with the others kernels. Instead of running one big kernel, three individual kernels are launched simultaneous. Dividing each kernel is possible to implement shared memory though each kernel which otherwise wasn't possible.

---

```
int i = blockIdx.x * blockDim.x + threadIdx.x + 2;
int j = blockIdx.y * blockDim.y + threadIdx.y;
int index = j * NXCUDA_CONST + i;

if (i > 1 && i < NX + 2 && j >= 0 && j < NY)
    deltam[index] = sfrelax[index] + sdex[index] + lapl[index] - sm[index];
```

---

LISTING 5.5: Evaluation of individual coordinates of the Zhang and Li model

This same method was applied to every kernel that was possible to separate into three kernels calls. Some kernels cannot be separate, such as the cross product, because, the cross product uses pinned memory block from the other streams. The figure 5.4 shows the results of concurrent kernels in the Tesla K20.

---

```
for (int i = 0; i < 3; i++)
    gsolution<<<blocks, threads, 0, stream[i]>>>(spinAccXYZ[i]->getDev_deltam(),
                                                       spinAccXYZ[i]->getDev_sfrelax(),
                                                       spinAccXYZ[i]->getDev_sm(),
                                                       spinAccXYZ[i]->getDev_sdex(),
                                                       spinAccXYZ[i]->getDev_lapl());
```

---

LISTING 5.6: Evaluate Zhang and Li model.



FIGURE 5.4: Concurrent kernels in the Tesla K20 using NVIDIA’s Visual Profiler.

Concurrent kernels demonstrates a very promising technique to achieve a huge performance increment in the current simulation. In theory is possible to have multiples kernels executing at the same. However, there are some downsides to this implementation; correctly synchronize kernels, waiting time and hardware resources are among the problems [21]. The timeline of the application 5.5 illustrates the waiting time between kernels execution. However, the waiting time are very small time steps between 0.01ms and 0.01ms, but waiting time occurs for each step of the RK4, appears approximate 45,00 times. Furthermore, branching the kernel execution process should eliminate the issue.

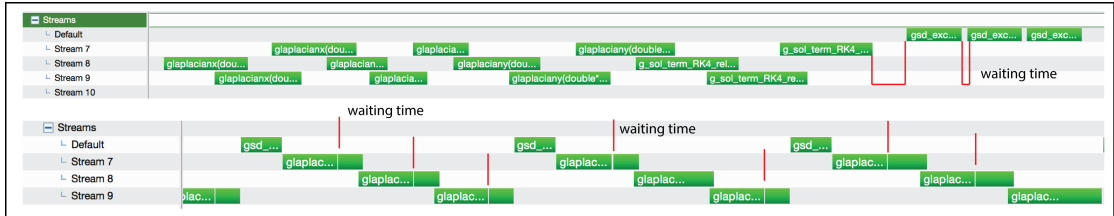


FIGURE 5.5: Waiting time between each concurrent kernel execution

### 5.2.3 Shared Memory

Shared memory is faster than global memory(read Chapter 4 for more reference), however, shared memory is very limited. To be able to implement shared memory in the

kernels, we needed the kernels to be separated in their x, y and z coordinate, as mentioned in the previous section. In addition, this allows us to implement shared memory across each kernel, otherwise wouldn't be possible. Shared memory was applied in all the kernels were global memory was used extensively. Eliminating the number clock cycles per thread.

The idea behind shared memory is to reduce the amount of global memory calls, which has about 400-600 clock cycles, while the shared memory only 1-32 clock cycles 4.4. The shared memory implementation is accomplish by allocating the data from the thread block into a temporary array, in other words the shared memory. In addition, the kernel is able to performed calculations on the temporary array and write the values onto the global memory. The implementation code is illustrated in the listing 5.7. There is no guaranty that threads will execute at the same order. Using `__syncthreads()` will wait until all threads have completed their task, in this case loading global memory into the shared memory array. Chapter 4 section thread synchronization, has more information about thread synchronization and shared memory. Once all the operations on the shared memory array are finish. The final part is to write the shared memory values back to the the global memory.

---

```

int i = blockIdx.x * blockDim.x + threadIdx.x;
int j = blockIdx.y * blockDim.y + threadIdx.y;
int index = j * NXCUDA_CONST + i;

if (i > 1 && i < NX + 2 && j >= 0 && j < NY){
    int cacheIdx = threadIdx.y * blockDim.x + threadIdx.x;
    __shared__ double deltamS[THREADS_SHARED * THREADS_SHARED];

    //load memory into shared memory
    deltamS[cacheIdx] = operationGlobal(globalMemory);
    __syncthreads();

    //copy back the shared memory to global memory
    deltam[index] = deltamS[cacheIdx];
}

```

---

LISTING 5.7: Shared memory

To calculate the laplacian we need to access a great amount of global memory, that is located near the value of interest. In this case a region of 4x4 grid. The figure 5.6 illustrates what part of the block is used for allocating shared memory and global memory. The global memory is used for the boundary conditions of the block, while the shared memory for all the values inside the block.

The code 5.8 demonstrates to how calculate the Laplacian from the equation 2.3 with the implementation of shared memory. First we load all the global memory into a temporary

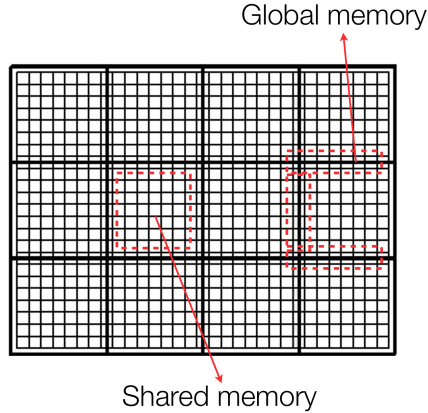


FIGURE 5.6: Shared Memory Strategy for Laplacian evaluation

array, the shared memory. Then we performed the calculation on the shared memory as mentioned before. Lastly return data to the global memory.

---

```

if (i >= 0 && i < NX && j >= 0 && j < NY){
    __shared__ double lapS[ THREADS_SHARED * THREADS_SHARED ];
    lapS[sIdx] = deltam[Index];
    __syncthreads();

    if (threadIdx.x >= 2 && i < threadIdx.x - blockDim.x - 2){ //shared
        lapy[idx] = - lapS[sIdx + 2] / 12.0 + 4.0 * lapS[sIdx + 1] / 3.0
                    - 5.0 * lapS[sIdx] / 2.0
                    - lapS[sIdx - 2] / 12.0 + 4.0 * lapS[sIdx - 1] / 3.0;
    } else{ //global memory
        lapy[idx] = - deltam[idx + 2] / 12.0 + 4.0 * deltam[idx + 1] / 3.0
                    - 5.0 * deltam[idx] / 2.0
                    - deltam[idx - 2] / 12.0 + 4.0 * deltam[idx - 1] / 3.0;
    }
}

```

---

LISTING 5.8: Laplacian evaluating using shared memory with boundaries condition

The current approach seems very promising for reducing global memory. However, great amount of time is spent on loading data onto the shared memory array, In consequence delaying threads executing, resulting a decrease in performance. Fast allocating shared memory data is the optimal solution to ensure the optimal use of this type of memory. The results of such implementation are in the following section, optimization results.

#### 5.2.4 Structure of Arrays, SAO

AoS and SoA refer to "Array of Structures" and "Structure of Arrays" respectively. These two terms refer to two different ways of laying out your data in memory. This is illustrated in figure 5.7 and 5.8 respectively. AOS, grouping properties of an object together and making an array of those objects in memory, whereas a structure of arrays

would be a single structure in which you make an array for each property. The structure of arrays can allow for better cache utilization, easier to access continues data, making better use of each read you make from memory, providing a more effective route to memory.

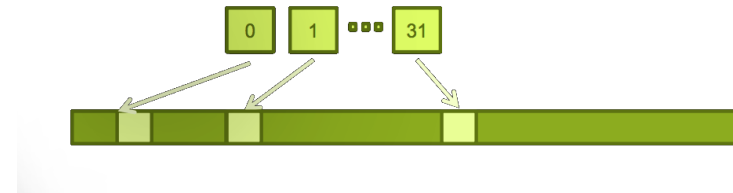


FIGURE 5.7: AOS memory layout

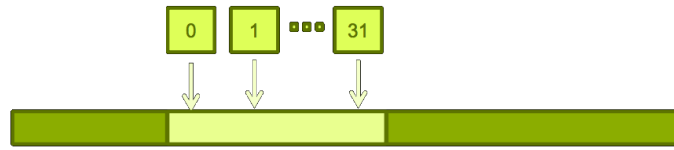


FIGURE 5.8: SAO memory layout

The initial implementation the x, y, z data was allocated in separated blocks. Furthermore when accessing blocks of the the same coordinates, the register access the data as the figure 5.7.

---

```
deltam_x = (double **)calloc(NYCUDA, sizeof(double *));
deltam_y = (double **)calloc(NXCUDA, sizeof(double *));
deltam_z = (double **)calloc(NXCUA, sizeof(double *));
```

---

LISTING 5.9: AOS implementation

To solve the issue, a custom class GPUMatrix was programmed. The class contained all the matrices for the device. Moreover, the classes allocated the data for each Matrix and free the memory automatically when the simulation is over. The was allocated in a structure that easier for the device to access common elements. For example, evaluating operations only on the x coordinate, the kernel physically access matrices that are near by. Eliminating unassary shift in registers, or hierarchy memory access.

---

```
GPUMatrix<T> *dev_deltam;
GPUMatrix<T> *dev_sdex; //Exchange term
GPUMatrix<T> *dev_sfrelax;
GPUMatrix<T> *dev_m;
```

---

LISTING 5.10: SOA implementation

The current approach eliminates unnecessary data shift in registers, and is able to stack more values per registers. In theory more computational time per threads. The results

of such implementation is illustrate on the last section of the chapter. With the new implementation the code become more readable for future improvements.

### 5.2.5 Occupancy

Firstly, we increased the use of constant memory in the device, eliminating redundant evaluations of variables and operations. The results are increase in performance and more computational workload on each thread. In addition, constant memory modifications are illustrated in the code [5.11](#). Matrix calculation for the boundary conditions [2.7](#) and [2.7](#) were implemented using constant Memory, reducing unnecessary calls in the device.

---

```
gsource << <blocks, threads >> >(u_val, dev_sm_z, dev_mz, NXCUDA);

sfrelax_y[index] = -deltam_y[index] / tau_sf;

DELTAX = (double)TX / (double)NX;
```

---

LISTING 5.11: Constant Memory changes

The different numbers of threads per block and as well the number of blocks per grid can dramatically increase or decrease the performance of the application. The table [5.5](#) illustrate the different threads per block configuration on the GeForce GTX 580. Using NVIDIA's Profiler is possible to obtain the occupancy percentage of threads the device. The initial configuration for the Fermi and the Kepler was 32x32 threads per block for global memory and 16x16 threads per block for the shared memory. We found, that the optimal configuration for the Fermi cards was 16x16 threads per block and as well for the shared memory and for the Kepler cards was 32x32 threads per block for both memory types.

| Threads | Shared | speedup | time    | Occupancy |
|---------|--------|---------|---------|-----------|
| 8x8     | 8x8    | 7.217x  | 52318.3 | 56.6%     |
| 16x16   | 8x8    | 7.625x  | 49517.3 | 86.6%     |
| 16x16   | 16x16  | 7.978x  | 47329.2 | 100.0%    |
| 32x32   | 16x16  | 7.356x  | 51333.4 | 66.6%     |
| 32x32   | 32x32  |         | Failed  |           |

TABLE 5.5: Threads per block configuration and occupancy on the Fermi architecture

## 5.3 Optimization results

This section is a overview of the optimization results compared with the initial CUDA implementation. Each version of the code is compared with the first test results. The

figure 5.9 and 5.10 illustrates the the time execution and the speedup respectively for the tables 5.6 and 5.7. The final version of the code is the Occupancy. Moreover, the greatest performance occurred on the GeForce GTX 580 Card with 8.0x speedup 5.10.

| GPU             | Original | Constant | Streams  | Shared  | SAO      | Occupancy |
|-----------------|----------|----------|----------|---------|----------|-----------|
| Tesla K20m      | 107322.7 | 101513.4 | 97106.0  | 90201.7 | 68988.2  | 66456.0   |
| Tesla M2070     | 110912.3 | 103212.4 | 130754.1 | 97343.4 | 73938.1  | 70299.3   |
| Tesla C2050     | 109635.1 | 101212.4 | 128516.6 | 96762.0 | 72964.5  | 69358.1   |
| GeForce GTX 580 | 70002.7  | 68712.2  | 76481.9  | 68567.1 | 51603.7  | 47213.2   |
| GeForce 650m    | 244372.9 | 237371.9 | 227237.8 | 279804  | 181217.4 | 174419    |

TABLE 5.6: GPU Optimization time

The table 5.6 displays the overall executing time for all the version of the code, original, constant, streams, shared memory, SAO and Occupancy. We can see compared the initial time and the final there is a difference between 40s and 50s time decrease. The time reduction is relatively low. There is no big difference in waiting 100s or 66s to a simulation to complete. However, if we increase the data set to five decimal points, the simulation can take up-to a couple of hours or days. Finally, the speedup comparison in table 5.7 and figure 5.10 illustrates how much performance increase we could obtain in a new simulation using the new implementation.

| GPU             | Original | Constant | Streams | Shared | SAO    | Occupancy |
|-----------------|----------|----------|---------|--------|--------|-----------|
| Tesla K20m      | 3.517x   | 3.718x   | 3.888x  | 4.186x | 5.473x | 5.682x    |
| Tesla M2070     | 3.403x   | 3.534x   | 2.888x  | 3.879x | 5.107x | 5.371x    |
| Tesla C2050     | 3.442x   | 3.571x   | 2.938x  | 3.902x | 5.175x | 5.444x    |
| GeForce GTX 580 | 5.391x   | 5.521x   | 4.937x  | 5.551x | 7.317x | 8.0x      |
| GeForce 670MX   | 1.544x   | 1.598x   | 1.662x  | 1.349x | 2.084x | 2.163x    |

TABLE 5.7: GPU Speedup performance

The table 5.11 illustrates the final profiling results using NVIDIA’s profiling tools. On the initial profiling ??, the Laplacian evaluation consumed about half of the overall simulation time. However, on the final optimization results 5.11, the Laplacian was reduced from 44.37% to 26.24 % on execution time. But more importantly the importance of the kernel was reduced, in other words more computational workload on the kernels. The same occurred for the Runge and Kutta term evaluation. The speedup mainly occurred in the Occupancy version of the code, see table 5.7. Furthermore, the *gsdExchangeFull* incremented from 13.37%. 23.35%, which is not necessary good. The increment in time is due to shift in streams operators, the *gsdExchangeFull* is processed in the default stream zero, while the others kernels launched concurrently in a different stream.

The Tesla K20m was the only GPU which in every code modification it did not lose performance over the course of the optimization process. However, the other GPUs

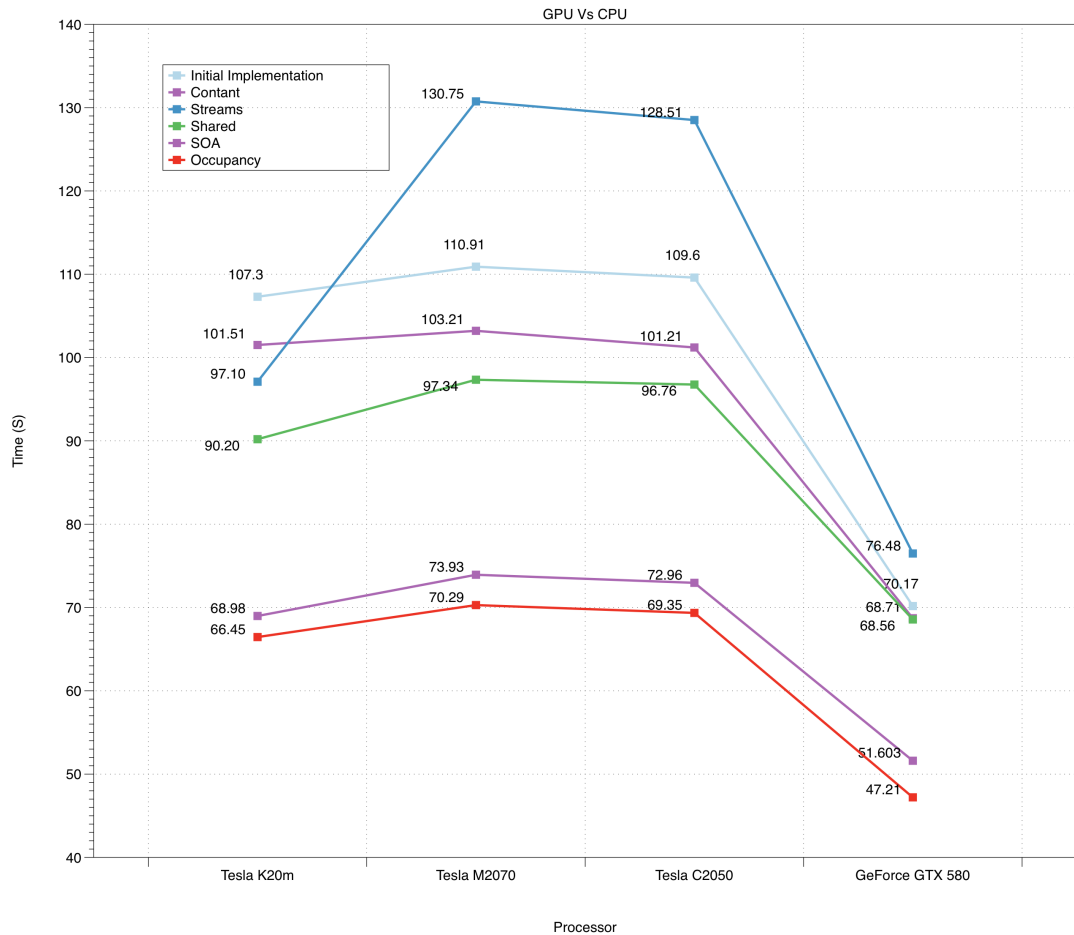


FIGURE 5.9: Overall simulation time

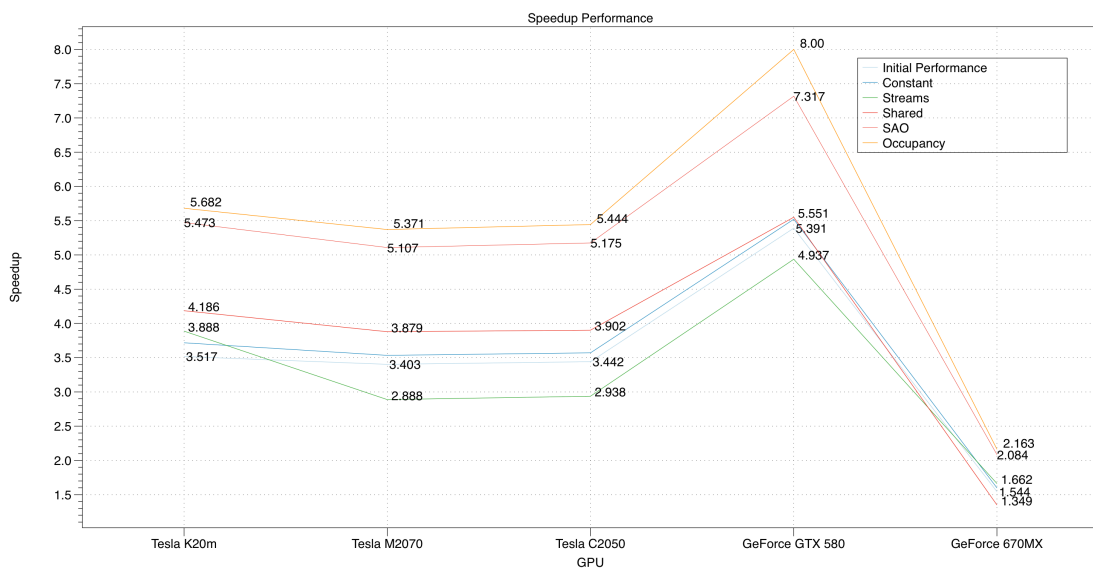


FIGURE 5.10: Speedup performance output.

| Time % | Time   | Calls  | Avg     | Kernel                         |
|--------|--------|--------|---------|--------------------------------|
| 35.24  | 21.33s | 216330 | 98.5us  | <i>gSolTermRK4Relaxation</i>   |
| 26.24  | 15.88s | 288441 | 55.0us  | <i>glaplacianXYBboundaries</i> |
| 23.35  | 14.13s | 160000 | 88.3us  | <i>gsdExchangeFull</i>         |
| 15.17  | 9.18s  | 72108  | 127.2us | <i>gSolTerm4RK4Relaxation</i>  |

FIGURE 5.11: Final optimization results using NVIDIA’s profiler, on the Tesla K20m

drop performance in the stream optimization stage. The stream process is where each kernel was divided into three separated kernels. Doing this we were able to calculate the x, y, z coordinates independently. In addition, this enable room to implement shared memory across possible kernels. The GPU table specifications 5.2 illustrates that the Tesla K20m is the only GPU card with CC of 3.5. This is important to mention, because the CC 3.5 has access to Hyper-Q technology. Moreover, Hyper-Q is able to synchronize automatically concurrent kernels, just by activated a steam process to the kernel.

The SOA optimization, improved overall dramatically the performance of the application, obtaining a 1.2x - 2.0x speedup in all GPU cards, see table 5.7 and figure 5.10. The final version, Occupancy, improved up-to 0.7x speedup on the 580 GPU. However, for the Teslas cards only 0.2x-0.25x speedup. The speedup difference, 0.5x, is due to the process cycle of the GeForce GPU.

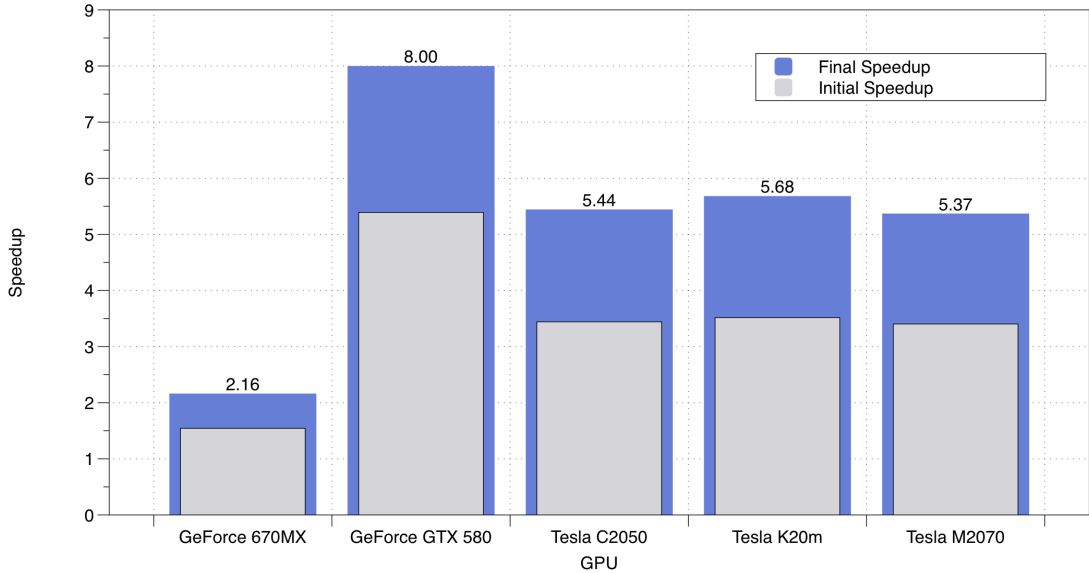


FIGURE 5.12: Optimization speedup overview

We expected that the newest card, the Tesla k20m, would obtain the highest speedup overall, certainly because it has more CUDA cores, the highest compute capabilities. However, if falls behind the GeForce 580 with about 2.5x speedup difference (table 5.7). In addition, the Tesla K20 only had a difference of 0.3x speedup compared with the

Teslas Cards, see figure 5.10 and 5.12. The GeForce compared with the others GPUs specifications has most Processor clock (GHz), more mathematical calculations per cycle, see table 5.2 for GPU specifications comparison. The results demonstrate the increase of workload and occupancy on the device. Increasing the computational process per thread and per block.

Finally, various techniques and practices from chapter 4 were used to archive speedup and increase performance. Techniques such as increase the use of constant memory, shared memory, changed the memory allocating access, analyzed thread branching and finally analyzed kernel occupancy. The highest performance of all GPUS did not occurred on the newest NVIDIA card, the K20m, which is the most expensive of all the GPUs. The actual improvement appeared on the GeForce 580 (the more GHz of all GPUs) with a 2.32x speedup difference in comparison with the Tesla K20m, table 5.10. If the problem data set is to be scaled, for example, to a simulation of 8 days, the speedup performance of 8.0x will drastically decrease the time execution in only one day. Moreover, is possible to execute more simulations on the initial time step.

## Chapter 6

# Conclusions and future work

GPUs definitely have a place in the world of computational physics and other similar applications, their use allows to do the same work with less energy and more science with less resources. They make HPC computing clusters affordable for small research groups. The true limit test of this new technology will be if it is actually used to advance new science. In the field of computational physics studies that do push the barrier of what is computationally feasible, from speedups of 1.5x to 20x using GPUs[20].

Acceptance has been slow due to many factors, GPUs are sometimes seen as a fad or a niche, the specialized skill set and effort required for GPU programming along with the risk of spending money to setup a GPU cluster, does raise a concern for productivity and viability of this technology. Adopting this technology requires abandoning legacy codes and smart optimizations that have been developed over the years. A wrong choice may result in wasted time and effort.

What is certain is at the moment, is the overall direction of the industry towards higher parallelism, as single threaded performance has reached a local limit, all types of processors are seeking more performance out of parallelism. This means that a large portion of the work needed to parallelize a code for a certain parallel architecture will most probably be applicable to another parallel architecture as well. From the literature and my experiences, one can observe that in order to achieve good results in programming with GPUs it is necessary to take a Heterogeneous approach to coding. That is adopting multi-threaded CPUs and concurrent GPU type algorithms.

Spintronics, in particular involves designing new magnetic materials for spin-devices and modeling and understanding of spin-transport at molecular and atomic scale. Manipulating magnetic domain walls to store and transfer information is envisioned to enable

high-density, low-power, non-volatile, and non-mechanical memory. Promising for future systems for example the racetrack memory by Parkin at IBM, where DWs can be moved by applied magnetic fields and/or by currents via the spin transfer torque effects such as the simulation proposed by this research. However, most of the technologies and experiments are still in developing. Furthermore, there are several obstacles to be overcome to enable these technologies.

Using computer simulation is possible to predict the outcome of the theoretical approach. In this case reproduce the effects of spin diffusion by numerically implementing the Zhang-Li model into micromagnetics, we apply a current to a regime of DWs in a NiFe soft nanostrips. Furthermore, providing the theoretical experiments with high precision on relative inexpensive computers. By using the highly parallel capabilities of the GPU it was possible to dramatically reduce the computation time of the simulation from around 400s on the CPU to 41s on a GPU. In other words upto a 8.0x speedup. With this result is possible to performed 10 times more simulations on the previous time step.

Through the optimization we achieved a maximum speedup of 8.0x. The result did not occurred on the newest device, the K20m. But on the mid-range GPU, the GeForce GTX 580, which has more clock cycles (GHz) than the others cards. The newest device, the K20m is 10 times more expensive than the 580 card. The tesla cards are mainly designed for server used, multiple users, while the GeForce for high performance graphics, high workload on a single user. The optimization approach was focused on giving more workload on the GPUs, more performance per SM and increasing the work of threads per block. Lastly, the GTX 580 is not the newest GeForce card available in the market, the new GeForce 980 is expected to have a 40% increase in performance over the 500 GTX series.

The simulations was performed on a relative small data set. However, it is possible to increase the data set, in other words, the magnetization data. Which overall will reduce the execution time by a factor of 8, increasing the number of simulations in the same time frame. Future test on the magnetization data can be performed on a newer GPU architecture, such as the Maxwell. For example, on the new GeForce 980 or on the Tesla K80.

The current thread is to push the hardware capabilities and performance along with Mooers' Law, despite these issues there are some trends in the hardware industry that will make working with GPU easier and more widespread within a HPC context:

### **3D Memory**

Stacks DRAM chips into dense modules with wide interfaces, and brings them inside the same package as the GPU. This lets GPUs get data from memory more

quickly boosting throughput and efficiency allowing us to build more compact GPUs that put more power into smaller devices. The result: several times greater bandwidth, more than twice the memory capacity and quadrupled energy efficiency.

### **NVLink**

Todays computers are constrained by the speed at which data can move between the CPU and GPU. NVLink puts a fatter pipe between the CPU and GPU, allowing data to flow at more than 80GB per second, compared to the 16GB per second available now.

### **Pascal Module**

NVIDIA has designed a module to house Pascal GPUs with NVLink. At one-third the size of the standard boards used today, theyll put the power of GPUs into more compact form factors than ever before.

### **Mobile and embedded Devices**

With the new Tegra K1 is possible to do supercomputing on the level of mobil devices, achieving upto 1 TFlops of performance. Embedded devices with CUDA capabilities is possible to integrate high performance algorithms to such small platforms.

### **Cloud Computing**

NVIDIA is pushing the limits of bring computer graphics to the cloud, the idea is for everybody have access to high quality computer graphics.

Using heterogenous computing is possible to dramatically decrease computational time on CPU applications that are not feasible with the current CPU paradigm. Leaving room for new types computational simulations in a reasonable accomplish time frame. To conclude, I offer my personal perspective on GPU computing. I think the importance of using accelerator hardware is an economic and environmental issue. The environmental aspect of doing computing is often overlooked, but an ever increasing important one. As heavy computer users we will have to take responsibility for our electricity use. The benefit of less energy use is clear with more computational power.

# Bibliography

- [1] D. C. R. A and M. D. S. B. Spin transfer torques, 711.
- [2] J. A. Anderson, C. D. Lorenz, and A. Travesset. General purpose molecular dynamics simulations fully implemented on graphics processing units. *J. Comput. Phys.*, 227(10):5342–5359, May 2008.
- [3] CentOS. Centos project. <http://www.centos.org/>, 2015, Cited January 2015.
- [4] S. Che, M. Boyer, J. Meng, D. Tarjan, J. Sheaffer, S.-H. Lee, and K. Skadron. Rodinia: A benchmark suite for heterogeneous computing. pages 44–54, 2009.
- [5] D. Claudio-Gonzalez, A. Thiaville, and J. Miltat. Domain wall dynamics under nonlocal spin-transfer torque. *Phys. Rev. Lett.*, 108:227208, Jun 2012.
- [6] S. Cook. *CUDA Programming: A Developer’s Guide to Parallel Computing with GPUs*. Morgan Kaufmann Publishers Inc., San Francisco, CA, USA, 1st edition, 2012.
- [7] J. Fagerberg, D. C. Mowery, and R. R. Nelson. *Handbook of magnetism and advanced magnetic materials*, volume 2. Wiley-Interscience, Chichester, Sep 2007.
- [8] R. Farber. *CUDA Application Design and Development*. Morgan Kaufmann Publishers Inc., San Francisco, CA, USA, 1st edition, 2011.
- [9] E. Golovatski. *Spin Torque and Interactions in Ferromagnetic Semiconductor Domain Walls*. BiblioBazaar, 2012.
- [10] T. H ö rmann. Gpu-optimised implementation of high-dimensional tensor applications. Master’s thesis, Institut für Informatik, Technische Universität München, Dec. 2014.
- [11] P. Haney and T. U. of Texas at Austin. Physics. *Spintronics in Ferromagnets and Antiferromagnets from First Principles*. University of Texas at Austin, 2007.
- [12] A. Harju, T. Siro, F. Canova, S. Hakala, and T. Rantalaiho. Computational physics on graphics processing units. 7782:3–26, 2013.

- [13] IMB. The application of spintronics. <http://www-03.ibm.com/ibm/history/ibm100/us/en/icons/spintronics/>, 2013, Cited January 2015.
- [14] G. Karapetrov and V. Novosad. Domain walls riding the wave. *Physics*, 3:96, Nov 2010.
- [15] D. B. Kirk and W.-m. W. Hwu. *Programming Massively Parallel Processors: A Hands-on Approach*. Morgan Kaufmann Publishers Inc., San Francisco, CA, USA, 1st edition, 2010.
- [16] R. Landaverde, T. Zhang, A. K. Coskun, and M. Herbordt. An investigation of unified memory access performance in cuda. 2014.
- [17] K.-J. Lee, M. Stiles, H.-W. Lee, J.-H. Moon, K.-W. Kim, and S.-W. Lee. Self-consistent calculation of spin transport and magnetization dynamics. *Physics Reports*, 531(2):89 – 113, 2013. Self-consistent calculation of spin transport and magnetization dynamics.
- [18] Z. Li and S. Zhang. Domain-wall dynamics and spin-wave excitations with spin-transfer torques. *Phys. Rev. Lett.*, 92:207203, May 2004.
- [19] J. Nickolls and W. J. Dally. The gpu computing era. *IEEE Micro*, 30(2):56–69, mar 2010.
- [20] NVIDIA. Popular gpu-accelerated applications. [http://www.nvidia.com/docs/I0/64497/NV\\_GPU\\_Accelerated\\_Applications.pdf](http://www.nvidia.com/docs/I0/64497/NV_GPU_Accelerated_Applications.pdf), 2012, Cited January 2015.
- [21] nVidia. *CUDA C Best Practices Guide*, Oct. 2014.
- [22] NVIDIA. Cuda documentation. <http://docs.nvidia.com/cuda/#axzz30RV92FoV>, 2014, Cited January 2015.
- [23] N. L. Oak Ridge. Titan. <https://www.olcf.ornl.gov/titan/>, 2013, Cited January 2015.
- [24] S. S. Parkin, M. Hayashi, and L. Thomas. Magnetic domain-wall racetrack memory. *Science*, 320(5873):190–194, 2008.
- [25] D. A. Patterson and J. L. Hennessy. *Computer Architecture: A Quantitative Approach*. Morgan Kaufmann Publishers Inc., San Francisco, CA, USA, 1990.
- [26] W. H. Press, S. A. Teukolsky, W. T. Vetterling, and B. P. Flannery. *Numerical Recipes in C (2Nd Ed.): The Art of Scientific Computing*. Cambridge University Press, New York, NY, USA, 1992.

- [27] C. Richard, M. Houzet, and J. Meyer. Andreev current induced by ferromagnetic resonance. *Phys. Rev. Lett.*, 109:057002, Jul 2012.
- [28] G. Ruetsch and M. Fatica. *CUDA Fortran for Scientists and Engineers: Best Practices for Efficient CUDA Fortran Programming*. Elsevier Science, 2013.
- [29] J. Sanders and E. Kandrot. *CUDA by Example: An Introduction to General-Purpose GPU Programming*. Addison-Wesley Professional, 1st edition, 2010.
- [30] J. B. Schneider. Understanding the finite-difference time-domain method, [www.eecs.wsu.edu/~schneidj/ufdtd](http://www.eecs.wsu.edu/~schneidj/ufdtd), 2010.
- [31] R. F. Service. What itll take to go exascale. *Science*, 335(January):394–396, 2012.
- [32] E. Tsymbal and I. Zutic. *Handbook of Spin Transport and Magnetism*. Taylor and Francis, 2011.
- [33] S. O. Valenzuela. Nonlocal electronic spin detection, spin accumulation and the spin hall effect. *International Journal of Modern Physics B*, 23(11):2413–2438, 2009.
- [34] C. Wang. Characterization of spin transfer torque and magnetization manipulation in magnetic nanostructures, 2012.
- [35] N. Whitehead and A. Fit-florea. Precision and performance: Floating point and ieee 754 compliance for nvidia gpus.
- [36] N. Wilt. *The CUDA Handbook: A Comprehensive Guide to GPU Programming*. Pearson Education, 2013.
- [37] V. Zayets. Spin and charge transport in materials with spin-dependent conductivity. *Phys. Rev. B*, 86:174415, Nov 2012.
- [38] S. Zhang and Z. Li. Roles of nonequilibrium conduction electrons on the magnetization dynamics of ferromagnets. *Phys. Rev. Lett.*, 93:127204, Sep 2004.